

11  
110202R  
199335  
71P

LIFT AUGMENTATION ON A DELTA WING  
VIA LEADING EDGE FENCES AND THE GURNEY FLAP

(NASA-CR-194793) LIFT AUGMENTATION  
ON A DELTA WING VIA LEADING EDGE  
FENCES AND THE GURNEY FLAP M.S.  
Thesis (California Polytechnic  
State Univ.) 71 p

N94-24103

Unclas

G3/02 0199885

by

Mark D. Buchholz

A thesis  
submitted in partial fulfillment  
of the requirements for the degree of  
Master of Science in the Department of Aeronautical Engineering  
California Polytechnic State University, San Luis Obispo  
December 1992

AUTHORIZATION FOR REPRODUCTION  
OF MASTER'S THESIS

I grant permission for the reproduction of this thesis in its entirety  
or in any of its parts, without further authorization from me.

Mark D. Buchholz  
Signature

12-3-92  
Date


APPROVAL PAGE

TITLE: Lift Augmentation on a Delta Wing via Leading Edge  
Fences and the Gurney Flap

AUTHOR: Mark D. Buchholz

DATE SUBMITTED: November 1992

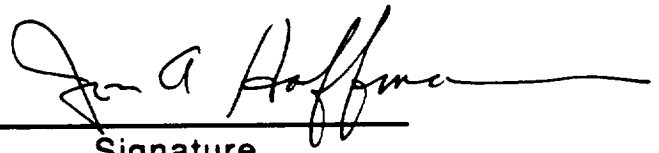
Jin Tso  
Advisor/Committee Chair

  
Signature

James C. Ross  
Committee Member

  
Signature

Jon A. Hoffmann  
Committee Member

  
Signature

## ABSTRACT

Lift Augmentation on a Delta Wing via Leading Edge Fences and the Gurney Flap

by

Mark D. Buchholz

Wind tunnel tests have been conducted on two devices for the purpose of lift augmentation on a  $60^\circ$  delta wing at low speed. Lift, drag, pitching moment, and surface pressures were measured. Detailed flow visualization was also obtained. Both the leading edge fence and the Gurney flap are shown to increase lift. The fences and flap shift the lift curve as much as  $5^\circ$  and  $10^\circ$ , respectively. The fences aid in trapping vortices on the upper surface, thereby increasing suction. The Gurney flap improves circulation at the trailing edge. The individual influences of both devices are roughly additive, creating high lift gain. However, the lower lift to drag ratio and the precipitation of vortex burst caused by the fences, and the nose down pitching moment created by the flap are also significant factors.

## ACKNOWLEDGMENTS

This work was made possible by NASA Grant NCC 2-730. The author wishes to thank Dr. Jin Tso, professor at Cal Poly, for his guidance, support, and enthusiasm throughout the project. Also, the author is indebted to his wife, Sandy, who provided emotional support and has shown great patience. Finally, the author thanks God for all the above blessings.

# TABLE OF CONTENTS

	Page
List of Figures . . . . .	viii
List of Symbols . . . . .	xi
Chapter	
1. Introduction . . . . .	1
Theory of Fence Vortex Trapping and Previous Work . . . . .	1
Gurney Flap Theory and Previous Work . . . . .	2
2. Apparatus and Procedure . . . . .	4
Test Models . . . . .	4
Force and Moment Measurements . . . . .	5
Vapor Flow Visualization . . . . .	5
Surface Oil Flow Patterns . . . . .	6
Pressure Measurements . . . . .	6
3. Leading Edge Fence Results and Discussion . . . . .	7
Effect of Fence Shape . . . . .	7
Effect of Fence Length . . . . .	8
Effect of Deflection Angle . . . . .	8
Effect of Fence Angle . . . . .	9
Hysteresis . . . . .	10

	Flow Visualization of the Vortex Core . . . . .	11
	Surface Flow Visualization . . . . .	12
	Surface Pressure Distributions . . . . .	14
	Effect of Sweep Angle . . . . .	15
4.	Gurney Flap Results and Discussion . . . . .	17
	Tapered Height Gurney Flap . . . . .	17
	Constant Height Gurney Flap . . . . .	18
	Combined Fence-Flap Configuration . . . . .	19
	Comparison of Devices . . . . .	19
5.	Conclusions . . . . .	20
	References . . . . .	58

## FIGURES

Figure	Page
1. Vortex Trapping on Infinite Wing with Fence and Cross-stream Suction . . . . .	21
2. Effect of Gurney Flap on Flow Conditions Around an Airfoil . . . . .	21
3. General Schematic of Wing Model with Tapered Fence and Constant Height Gurney Flap . . . . .	22
4. Isometric Views of Delta Wing with Fences and Flap . . . . .	22
5. Model A, Main Test Model . . . . .	23
6. Model B, Surface Pressure Model . . . . .	23
7. Models with Varied Sweep Angle . . . . .	24
8. Effect of Fence Shape on Lift and Drag Coefficients . . . . .	25
9. Effect of Fence Length on Lift and Drag Coefficients . . . . .	26
10. Effect of Deflection Angle on Lift and Drag Coefficients . . . . .	27
11. Effect of Fence Angle on Lift and Lift Gain . . . . .	28
12. Effect of Fence Angle on Drag and Drag Gain. . . . .	29
13. Effect of Fence Angle on Lift to Drag Ratio . . . . .	30
14. Effect of Fence Angle on Pitching Moment . . . . .	30
15. Hysteresis of the Lift Coefficient . . . . .	31



16.	Vapor Patterns on 60° Delta Wing; Re = 430,000 . . . . .	32
17.	Vapor Patterns on 60° Delta Wing with $\phi = 5^\circ$ Fences; Re = 430,000 . . . . .	35
18.	Typical Crossflow Patterns Above 60° Delta Wing; $\alpha \approx 10^\circ$ . . . . .	38
19.	Oil Patterns on 60° Delta Wing; Re = 600,000 . . . . .	39
20.	Oil Patterns on 60° Delta Wing with $\phi = 5^\circ$ Fences; Re = 600,000 . . . . .	41
21.	Oil Patterns on $\phi = 5^\circ$ Fence; Re = 600,000 . . . . .	43
22.	Typical Crossflow Patterns Above 60° Delta Wing with Fences; $\alpha \approx 0^\circ$ . . . . .	44
23.	Surface Pressure Distributions; Re = 790,000 . . . . .	45
24.	Lift and Drag of Delta Wings of Various Sweep Angle . . . . .	49
25.	Gain in Lift and Drag with Fences on Delta Wings of Various Sweep Angle . . . . .	50
26.	Lift and Drag for Tapered Height Gurney Flap . . . . .	51
27.	Lift and Drag Comparison of Constant Height and Tapered Height Gurney Flaps . . . . .	52
28.	Lift and Lift Gain for Constant Height Gurney Flap . . . . .	53

29.	Drag and Drag Gain for Constant Height Gurney Flap . . . . .	54
30.	L/D for Constant Height Gurney Flap . . . . .	55
31.	Pitching Moment for Constant Height Gurney Flap . . . . .	55
32.	Effect of Gurney Flap on Oil Patterns on 60° Delta Wing; $Re = 600,000$ . . . . .	56
33.	Gain in Lift and Drag for Combined Fence-Flap Configuration . . . . .	57

## SYMBOLS

Symbol	Definition
$c$	local airfoil chord
$C_D$	drag coefficient, $D/q_\infty S$
$C_L$	lift coefficient, $L/q_\infty S$
$C_M$	pitching moment coefficient, $M/q_\infty S c_r$ , about 25% m.a.c.
$C_p$	pressure coefficient, $(p - p_\infty)/q_\infty$
$c_r$	wing root chord
$D$	drag force
$h$	height of device
$L$	lift force
$M$	pitching moment
m.a.c.	mean aerodynamic chord
$p$	surface static pressure
$p_\infty$	freestream static pressure
$q_\infty$	freestream dynamic pressure, $\rho U_\infty^2 / 2$
$Re$	Reynolds number, $\rho U_\infty c_r / \mu$
$S$	reference area, wing area + any projected device area
$t$	maximum wing thickness
$U_\infty$	freestream velocity

$x$	chordwise coordinate
$y$	spanwise coordinate
$\alpha$	angle of attack
$\Delta$	gain in force coefficient from device (i.e. $\Delta C_L, \Delta C_D$ )
$\delta_f$	flap deflection angle (i.e. $-90^\circ$ for perpendicular fence)
$\phi$	fence angle, smallest interior angle of tapered fence geometry
$\Lambda$	wing leading edge sweep angle
$\mu$	absolute viscosity
$\rho$	density

## CHAPTER 1

### Introduction

Delta wings of low aspect ratio have long been used for supersonic aircraft because of their favorable wave drag characteristics. In low speed conditions, the delta wing can still generate the necessary lift through a high angle of attack. This is due in part to the leading edge separation which rolls up into vortices above the wing. The vortices create high suction regions near the leading edge, as well as maintaining attached flow inboard.

A variation of the delta wing will be used by the proposed High-Speed Civil Transport (HSCT) which is required to fly at low angles of attack during takeoff and landing in order to avoid tail strike and impairment of the pilots' view. Therefore, a means must be developed to enhance the lift of delta wings at low angles of attack. Leading edge fences and Gurney flaps are two devices which can achieve this goal.

#### Theory of Fence Vortex Trapping and Previous Work

Using conformal mapping solutions, Rossow<sup>1-3</sup> suggested that vortices could be trapped above an infinite wing with a fence positioned near the leading edge, and cross-stream suction applied. See Figure 1. The trapped vortex would add apparent thickness and camber to the wing, thereby increasing lift. A rear fence could also be employed to aid in trapping the vortex and reduce the required cross-stream suction. Water channel and wind tunnel experiments<sup>4,5</sup> have supported these concepts. Rossow further

speculated on the application of vortex trapping to delta wings<sup>3</sup>, where the freestream velocity component parallel to the leading edge would provide the necessary "cross-stream suction". In an experimental study, Marchman<sup>6</sup> was able to trap vortices on a 75° delta wing through the use of inverted leading edge vortex flaps. For inverted deflections to 40°, increases in lift coefficient up to 0.18 were observed. In addition, a tapered flap was found to be superior to a constant chord flap.

Short fences near the apex region of delta wings have also been tested<sup>7,8</sup>. However, their usefulness is mostly in pitch and roll control, rather than lift augmentation.

Thus, tapered fences spanning the entire leading edge should provide high lift gain.

#### Gurney Flap Theory and Previous Work

The original Gurney flap was located at the trailing edge of a rectangular race car wing. It was a flat plate deflected 90°, perpendicular to the airfoil chord line. The flap chord was typically 1% to 5% of the airfoil chord. According to Liebeck<sup>9</sup>, race car testing by Gurney demonstrated improved downforce with the flap. Drag was also increased for the larger flap chords, but a reduction in drag was noticed for flap chords below 2%. Liebeck hypothesized that with the addition of the flap, separation of the upper surface flow was delayed, allowing for a wake momentum deficit of similar, even lower, magnitude than that of the bare airfoil. See Figure 2. Water tunnel dye flow experiments<sup>10</sup> and two-dimensional numerical

solutions<sup>11</sup> have supported this hypothesis. Experiments with a 5% Gurney flap on a two-element airfoil have also been conducted<sup>12</sup>. Higher lift and lower L/D were recorded, which is consistent with Liebeck's findings for larger flap chords.

Although the flow over a delta wing is not two-dimensional, the Gurney flap should still increase the circulation at the trailing edge, thereby increasing lift.

## CHAPTER 2

### Apparatus and Procedure

The experiment was conducted in the 3 x 4 ft. low-speed wind tunnel in the Aerodynamics Laboratory at CAL POLY.

#### Test Models

Figure 3 shows a schematic of the general delta wing model. All models were made of clear acrylic. The leading edges were beveled at 45° and the trailing edge was left blunt. The fences and flaps were made of 1/8 inch thick acrylic with sharpened edges. An isometric view of the attached tapered fences and Gurney flap is shown in Figure 4. The specific delta wing models used are shown in Figures 5 to 7.

Figure 5 shows a schematic of Model A, with 60° leading edge sweep. It was used for most force and moment measurements, and for vapor flow visualization.

Model B, used for surface pressure measurements, was geometrically similar and is pictured in Figure 6. The fences had an included angle of 5°, and were 1/4 inch thick. Nine rows of 0.01 inch diameter static pressure ports were located at 10% root chord intervals. The aft rows contained 20 ports on the wing semi-span and 7 ports on each side of the fence. The resolution decreased near the apex region. Clear flexible PVC tubing inside the wing connected each port to a pressure tap on the trailing edge. This model was also used for force measurements when the flap deflection angle of the leading edge fence,  $\partial_f$ , was greater than -90°.



Three additional models were used to test the effects of sweep angle. See Figure 7. The models were made slightly smaller in order to accommodate the  $\Lambda = 45^\circ$  wingspan in the test section. Models C, D, and E ( $\Lambda = 45^\circ, 60^\circ,$  and  $75^\circ$ ) were 1/2 inch thick, keeping the thickness ratio similar to the larger models. Model D was also used for surface oil flow patterns.

#### Force and Moment Measurements

Lift, drag, and pitching moment were measured using an Aerolab six-component sting balance. The strain gauge outputs were sent through an HP 3421A data acquisition control unit and read by an HP150 personal computer which time averaged 30 readings taken over a 10 second period. Non-dimensional coefficients were based on wing area plus the projected fence area (0 for  $\partial_f = -90^\circ$ ). The gain in non-dimensional force coefficient (i.e.  $\Delta C_L, \Delta C_D$ ) was defined as the coefficient of the bare delta wing subtracted from the coefficient of the delta wing with fence or flap. Pitching moment was taken about the 25% mean aerodynamic chord. For the majority of measurements, the uncertainties in lift and drag coefficient are at most  $\pm 0.01$ . The pitching moment coefficient has an uncertainty of less than  $\pm 0.005$ .

#### Vapor Flow Visualization

Vapor was generated by superheating a fogging fluid designed for theatre stage fogging machines. For heating, an electric current was passed through a 1/32 inch ID steel tube which also carried the

fluid. The outlet was positioned near the apex of the delta wing to allow entrainment of the vapor into the vortex core.

#### Surface Oil Flow Patterns

Surface flow patterns were generated by the oil film technique. A mixture of black powdered tempera paint and mineral oil was applied evenly to the white model surface. The wind tunnel was brought quickly up to the test speed, and ran until the coating of oil became too thin to flow.

#### Pressure Measurements

Surface pressures were measured using a 48 port Scanivalve® (model#48J9 2373) with a single pressure transducer rated for a maximum of 0.5 psig. The transducer output was read by an RC Electronics ISC-16 data acquisition system and processed by an Everex 386 personal computer which time averaged 256 readings taken over a 2 second period. Each row of pressure ports was scanned at several angles of attack. The accuracy for angle of attack is within  $\pm 0.1^\circ$ .

## CHAPTER 3

### Leading Edge Fence Results and Discussion

The first purpose of the fence study was to find a size and simple shape for the leading edge fence which would create a high lift increase without a substantial drag penalty. These parameters were refined to some degree. The second purpose was to examine the flow characteristics of one configuration in detail. This included vapor flow visualization, surface oil flow patterns, and surface pressure measurements. Additionally, the effect of leading edge sweep angle was briefly examined.

In the following results, it is noted that the base delta wings generated a higher lift curve slope than that reported by previous investigators<sup>13,14</sup>. The difference is readily explained by the 45° beveled leading edges and blunt trailing edge of the present test models, compared to the models of previous studies which had small bevels on all edges. Alterations to the present models, such as beveling the trailing edge at 45° or inverting the wing, reduced the lift curve slope to a value closer to previous studies. No wall corrections were made, since using smaller wings showed no change in the force and moment coefficients.

#### Effect of Fence Shape

Plots of  $C_L$  and  $C_D$  versus  $\alpha$  for tapered and rectangular fence configurations are shown in Figure 8. A tapered fence and a rectangular fence of equal area are compared. Both fences increase

the lift and drag over the bare delta wing, but the tapered fence produces higher lift as well as lower drag.

One noticeable difference between the fences is that the tapered fence allows flow to pass freely down the center of the delta wing, while the rectangular fence blocks the flow at the apex. To alleviate this difference, the forward 10% of the rectangular fence was removed. The lift and drag characteristics are somewhat altered, but the tapered fence remains superior.

#### Effect of Fence Length

The length of the tapered,  $\phi = 5^\circ$ , fence was shortened 25% from the trailing edge, and is compared to the full length fence in Figure 9. Both  $C_L$  and  $C_D$  are lower for the shorter fence. A better comparison can be made to the tapered,  $\phi = 2^\circ$ , full length fence which has nearly the same lift as the shortened fence, but much less drag. This demonstrates that the full length fence is more efficient at generating lift.

#### Effect of Deflection Angle

Figure 10 shows the plots of  $C_L$  and  $C_D$  versus  $\alpha$  at various deflection angles. When the fence is tilted outward from  $\partial_f = -90^\circ$ , there is little change in  $C_L$ , while  $C_D$  is slightly lower. This results in a higher lift to drag ratio. Also, since the aerodynamic coefficients are based on wing area plus fence projected area, the tilted fence has a greater actual lift force. Therefore tilting the fence creates a more efficient configuration. For simplicity, however, this study focuses on the perpendicular fence.

### Effect of Fence Angle

The included fence angle,  $\phi$ , was varied from  $2^\circ$  to  $8^\circ$ . Plots of  $C_L$  and  $\Delta C_L$  versus  $\alpha$  are shown in Figure 11. Greater lift corresponds to higher fence angles, and shifts in the lift curve of  $2^\circ$  to  $5^\circ$  are obtained. Lower fence angles exhibit a linear behavior with angle of attack similar to the bare delta wing. The higher fence angles show an anomaly near  $\alpha = 5^\circ$ , seen as a short plateau in lift coefficient for  $\phi = 5^\circ$  and a pronounced dip for  $\phi = 8^\circ$ . Also, the slope of the lift curve drops when the angle of attack exceeds  $5^\circ$ . The anomaly is emphasized by  $\Delta C_L$ . In general,  $\Delta C_L$  increases with angle of attack below  $\alpha \approx 5^\circ$  and then decreases. At any one angle of attack,  $\Delta C_L$  is roughly linearly proportional to the fence angle. The data presented was measured with increasing steps through angle of attack. Lower values, not plotted, are obtained near the anomaly with decreasing steps through angle of attack. This hysteresis loop will be examined in detail in the next section.

Figure 12 shows the plots of  $C_D$  and  $\Delta C_D$  versus  $\alpha$ . Higher fence angles produce higher drag. The anomaly at  $\alpha \approx 5^\circ$  is apparent in the drag coefficient for the higher fence angles. However, it is less distinct, as seen in the plots of  $\Delta C_D$ . Drag gain increases until  $\alpha \approx 5^\circ$ , then remains nearly constant.

A comparison of lift to drag ratio plots versus lift coefficient is presented in Figure 13. For positive lift coefficients, the bare delta wing has the highest L/D, with a peak of 5.2 at  $C_L = 0.4$ . The ratio decreases with increasing fence angle.

Plots of pitching moment versus angle of attack are shown in Figure 14. The moment coefficient is not appreciably changed with the addition of the fences.

### Hysteresis

Figure 15 shows the hysteresis in the  $C_L$  versus  $\alpha$  plot for the  $\phi = 5^\circ$  fence at  $Re = 860,000$ . The hysteresis loop exists between  $\alpha = 3^\circ$  and  $\alpha = 7^\circ$ . The upper and lower portions of the loop are data measured at steps through increasing and decreasing angle of attack, respectively. Note that upon entering the loop from either side, the lift curve slope is preserved. The change in lift curve slope across the hysteresis region suggests that the flow characteristics are different for  $\alpha < 3^\circ$  and  $\alpha > 7^\circ$ . It also appears that these characteristics can be carried into the hysteresis region. Flow visualization, presented in the following section, reveals that the characteristic difference is the absence or presence of vortex bursting over the wing. This is consistent with previous delta wing vortex bursting studies<sup>13</sup>, which showed a drop in the lift curve slope when the point of vortex bursting moved forward of the wing's trailing edge.

The angle of attack at which the vortex bursting occurs above the wing is also Reynolds number dependent. At a lower Reynolds number of 509,000, it occurs at a  $2^\circ$  higher angle of attack than for  $Re = 860,000$ . Similarly, it is expected that bursting will occur above the wing at lower angles of attack for higher Reynolds numbers.

### Flow Visualization of the Vortex Core

Figures 16 and 17 show one-half of the  $60^\circ$  delta wing with the vortex core highlighted by fogging fluid vapor. The bare delta wing at increasing angles of attack is pictured in Figure 16. At  $\alpha = 0^\circ$ , there is little sign of a vortex, as expected. The vortex is beginning to form at  $\alpha = 3^\circ$ , and the core is well defined at  $\alpha = 6^\circ$  and  $10^\circ$ . The picture at  $\alpha = 14^\circ$  reveals bursting of the vortex core above the aft portion of the wing. The bursting point moves farther forward with increasing angle of attack. For  $\alpha = 20^\circ$ , the bursting point has moved over half-way up the wing. This typical behavior has been well documented<sup>13-15</sup>.

Figure 17 records the effect on the vortex core at increasing angles of attack with the addition of  $\phi = 5^\circ$  fences. At  $\alpha = 0^\circ$  the vortex core is very distinct, with a slight kink above the aft portion of the wing. The cases for  $\alpha = 3^\circ$  and  $6^\circ$  appear similar. However, for  $\alpha = 6^\circ$ , the bursting of the vortex core could be seen approximately  $1/3$  of a root chord behind the trailing edge. The bursting point would remain there for long periods of time (30 to 60 seconds), but would occasionally move up to the trailing edge and back again. This occasional flow condition is also shown in the figure. For  $\alpha = 10^\circ$ , the bursting point remained above the wing in a steady location.

### Surface Flow Visualization

A typical cross flow pattern above a delta wing, perpendicular to the root chord, is shown in Figure 18 in order to clarify the following descriptions of the surface flow patterns.

Figures 19 and 20 present surface oil patterns on one half of the 60° delta wing. Figure 19 shows the patterns for the bare delta wing through increasing steps of angle of attack. At  $\alpha = 0^\circ$ , the flow separates from the leading edge due to local negative camber created by the beveled edge. Evidence of small vortex formations can be seen near the leading edge, with oil streaks in the outboard direction and a separation line visible. In addition, vortices appear to be turned downstream at several spanwise intervals. At  $\alpha = 3^\circ$ , the leading edge separation reattaches roughly along a ray of the delta wing. The flow passes straight back inboard of the reattachment line, while flow on the outboard side is dominated by the primary vortex. The secondary separation line is distinct near the apex but loses clarity downstream. Also, the vortex swirl angle at the surface is reduced on the aft portion of the wing, signaling a weak vortex. In contrast, at  $\alpha = 6^\circ$  the vortex appears strong, with a clear ray-like secondary separation line. The reattachment line of the secondary separation and the pattern of a weak secondary vortex are just visible. At  $\alpha = 10^\circ$ , the primary vortex pattern is farther inboard, and the secondary vortex pattern is distinct. The secondary separation line bends outboard near the trailing edge, perhaps due to vortex bursting aft of the trailing edge. The tertiary separation line



is now visible. Between the tertiary and secondary separation lines exists a "braided" pattern, which might be produced by a double-helix instability in the tertiary vortex core. This type of vortex instability, seen in swirling flows, was first documented by Sarpkaya<sup>16</sup>.

Figure 20 shows the surface patterns with the addition of the  $\phi = 5^\circ$  fences. At  $\alpha = 0^\circ$ , the primary vortex pattern is well established, and the pattern of the secondary vortex is adjacent to the fence. A large region between the two vortices contains the braided pattern. The case for  $\alpha = 3^\circ$  is very similar. At  $\alpha = 6^\circ$ , the secondary separation line bends outboard, affected by vortex bursting at the trailing edge. At  $\alpha = 10^\circ$ , the primary vortex pattern expands at the aft portion of the wing due to vortex bursting. The region between the primary and secondary vortices is diminished.

Surface patterns on the  $\phi = 5^\circ$  fences are pictured in Figure 21 for  $\alpha = 0^\circ$  and  $\alpha = 10^\circ$ . At  $\alpha = 0^\circ$ , the outboard side of the fence shows the flow attachment line in the middle of the fence, except near the apex where it gradually drops below the fence. The inboard side shows the reattachment line of the secondary separation and the secondary vortex pattern on the bottom half of the fence. The upper half of the fence shows the pattern of the primary vortex and the induced secondary separation line near the top of the fence. At  $\alpha = 10^\circ$ , the view of the outboard side of the fence shows the attachment line below the fence, with a gradual rise from apex to trailing edge. The inboard side of the fence shows little change in

the vortex patterns, except that the secondary separation line is not present.

Figure 22 presents a crossflow pattern above a delta wing with fences, which was derived from the oil flow and vapor patterns.

The oil flow patterns provided an average direction of the surface velocities. To see the instantaneous velocity directions, especially near vortex bursting, tufts were used on the wing surface. Due to their size and spacing, the tufts showed much less detail, but the effect of the primary vortex was easily seen. The  $60^\circ$  delta wing with  $\phi = 5^\circ$  fences was swept through increasing and decreasing angle of attack at  $Re = 860,000$ . For increasing angle of attack, the tufts showed steady flow patterns until the angle of attack reached  $6^\circ$ . Here, the tufts began to jitter in the vortex region at the trailing edge. This jittering, between the spanwise and chordwise directions, progressed up the wing with increasing angle of attack. When the angle of attack was decreased, the jittering retreated toward the trailing edge. But, it did not leave the wing until the angle of attack went below  $4^\circ$ , demonstrating the hysteresis in vortex bursting location.

#### Surface Pressure Distributions

Surface pressures were plotted for one half of the  $60^\circ$  delta wing upper surface and on both sides of the  $\phi = 5^\circ$  fence in Figure 23. The pressures on the bare delta wing and the delta wing with fences are compared at several increasing angles of attack. Generally, the

suction on the bare delta wing increases with angle of attack. It is highest near the apex and gradually decreases toward the trailing edge. The gradual buildup of the strong leading edge vortices can be seen as angle of attack increases from  $0^\circ$  to  $10^\circ$ . The high suction peaks near the leading edge are associated with the primary and secondary vortices. The inboard region of the wing has substantially less suction than the region under the vortices. Between these regions exists a dip in suction attributed to the reattachment of the primary separation.

In general, the addition of the fences creates strong primary and secondary vortices which impose clear suction peaks on the wing and fence surfaces. Also, a large pressure difference across the fence is evident. This is primarily responsible for the drag increase. In comparison to the bare delta wing, large increases in suction are present at  $\alpha = 0^\circ$  and  $3^\circ$ , where the bare delta wing vortex is very weak. At  $\alpha = 6^\circ$  and  $10^\circ$ , the fences still provide a large increase in suction on the forward portion of the wing. However, there is a loss of suction on the aft portion of the wing due to vortex bursting.

#### Effect of Sweep Angle

Plots of  $C_L$  and  $C_D$  versus  $\alpha$  for delta wings with leading edge sweep angles of  $45^\circ$ ,  $60^\circ$ , and  $75^\circ$  are shown in Figure 24. For the range of angle of attack tested, increasing the sweep angle lowers  $C_L$  and  $C_D$ , and delays vortex bursting. The resulting  $\Delta C_L$  and  $\Delta C_D$  from the  $\phi = 5^\circ$  fence are plotted in Figure 25. For  $\Lambda = 45^\circ$ ,  $\Delta C_L$

dropped off quickly with angle of attack due to vortex bursting, and the fence actually decreases lift for  $\alpha > 10^\circ$ . Comparison is made to the previous  $\Lambda = 60^\circ$  case, which shows vortex bursting to be delayed until  $\alpha \approx 7^\circ$  at this lower Reynolds number. For  $\Lambda = 75^\circ$ , the lift increase is lowest.  $\Delta C_D$  roughly decreases with increasing sweep angle. Overall, the leading edge sweep angle dramatically effects the performance of the fence.

## CHAPTER 4

### Gurney Flap Results and Discussion

This study also examined the Gurney Flap, a simple trailing edge device. Flap shape and size were examined, and surface oil flow patterns were compared. Finally, results from a combined fence-flap configuration are presented, and a comparison is made between the devices.

#### Tapered Height Gurney Flap

Following the two-dimensional theory of the Gurney flap, the flap height should be a percentage of the local airfoil chord. The resulting  $C_L$  and  $C_D$  for two such tapered height flaps are shown in Figure 26. Both the lift and drag increase with increasing height. The two-dimensional theory predicted that a small flap,  $h/c < 0.02$ , could reduce the drag. However, this could only occur if the flap were delaying separation on the upper surface. Oil patterns of the bare delta wing show no flow separation between the primary vortices. Therefore, even small Gurney flaps should increase the wake momentum deficit, producing more drag.

A comparison was made of the  $0.05c$  tapered and the  $0.02c_r$  constant height Gurney flaps. Plots of  $C_L$  and  $C_D$  versus  $\alpha$  are shown in Figure 27. The constant height flap produced nearly the same lift and drag as the tapered height flap. Also, the constant height flap is more attractive because of greater simplicity, less area, and less maximum height.

### Constant Height Gurney Flap

Plots of  $\Delta C_L$  and  $\Delta C_D$  versus  $\alpha$  are shown in Figure 28 for the constant height flap. Lift increases with increasing flap height, and shifts in the lift curve of  $4^\circ$  to  $10^\circ$  are obtained. A change in the lift curve slope signals vortex bursting which occurs at lower angles of attack with larger flaps. This behavior was not expected, since the flap decreases the adverse pressure gradient. However, experiments with swirling flows conducted by Sarpkaya<sup>16,17</sup> showed that high swirl angle as well as adverse pressure gradient will cause vortex breakdown. The flap, creating a high pressure region on the lower wing surface, could cause additional flow to circulate around the leading edges, thereby increasing the vortex swirl angle. The net effect of reducing the adverse pressure gradient while increasing the swirl angle adds instability in this case.

Figure 29 compares plots of  $C_D$  and  $\Delta C_D$  versus  $\alpha$ . Drag increases with increasing flap height. The lift to drag ratio is plotted versus lift coefficient in Figure 30. For the higher lift coefficients the flapped configurations exceed the bare delta wing in efficiency. However, the flap also generates a high negative pitching moment, as shown in Figure 31.

Surface oil patterns revealed no significant change with the addition of the flap, except near vortex bursting. Figure 32 compares the oil patterns at  $\alpha = 10^\circ$  for the delta wing and the delta wing with flap. With the flap, the secondary separation line bends outboard near the trailing edge due to vortex bursting.

### Combined Fence-Flap Configuration

The  $\phi = 5^\circ$  fences and the  $h = 0.01c_r$  flap produce comparable lift increases. Figure 33 plots  $\Delta C_L$  and  $\Delta C_D$  versus  $\alpha$ . Also, the results of the two devices combined are shown and compared to additive references. It is evident that both  $\Delta C_L$  and  $\Delta C_D$  are roughly additive for a combined configuration. However, the angle of attack for vortex bursting at the trailing edge is lowered.

### Comparison of Devices

The tapered fence and Gurney flap both increased the lift on the  $60^\circ$  delta wing, but the flap showed greater efficiency. Compared to the bare delta wing, the fence reduced the lift to drag ratio, while the flap increased the ratio at high lift coefficients. Both devices lower the angle of attack at which vortex bursting reaches the trailing edge, with the fence having much more effect than the flap. This is undesirable, since vortex bursting contributes to the stability problem of wing rock. The effect on pitching moment is another concern. The fences produce very little change in the pitching moment, while the flap creates a significant nose down moment.

## CHAPTER 5

### Conclusions

The lift on a  $60^\circ$  delta wing at low speed can be augmented by either tapered leading edge fences or the Gurney flap. The fences aid in trapping the vortices to increase suction on the upper surface, while the Gurney flap improves circulation at the trailing edge. Shifts in the lift curve as high as  $5^\circ$  and  $10^\circ$  were achieved by the fences and flap, respectively. The individual influences of both devices are roughly additive, creating high lift gain. However, the fences reduce L/D and precipitate vortex bursting. The flap significantly increases nose down pitching moment.



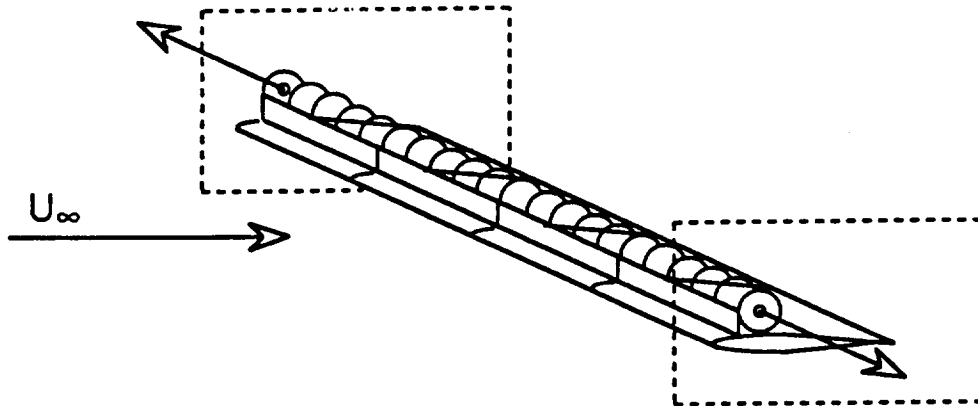


Figure 1. Vortex trapping on Infinite Wing with Fence and Cross-stream Suction.

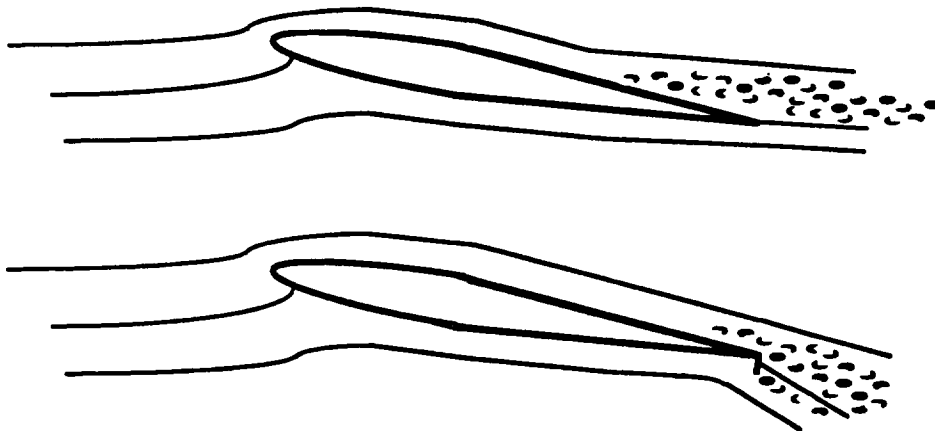


Figure 2. Effect of Gurney Flap on Flow Conditions Around an Airfoil.

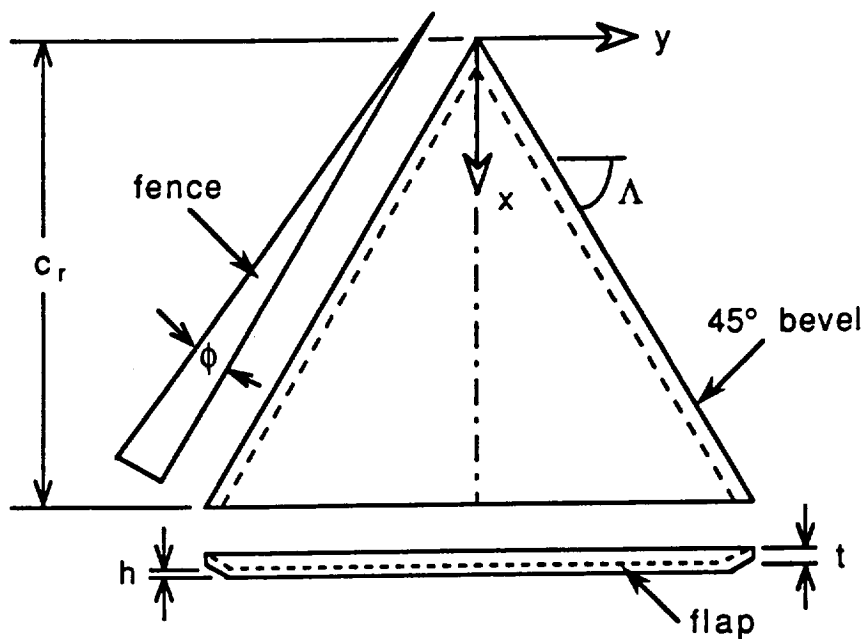


Figure 3. General Schematic of Wing Model with Tapered Fence and Constant Height Gurney Flap.

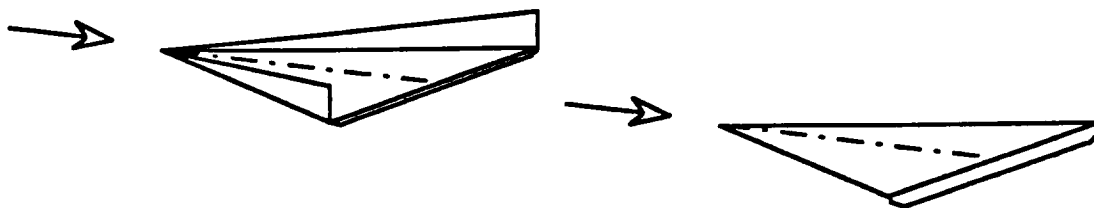


Figure 4. Isometric Views of Delta Wing with Fences and Flap.

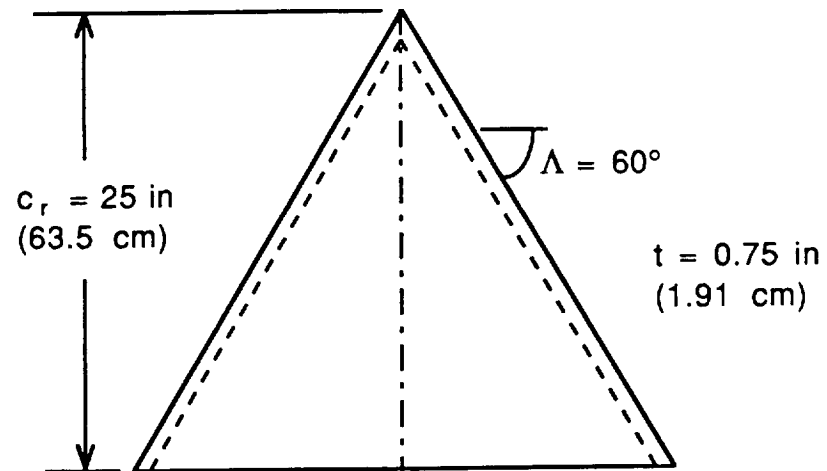


Figure 5. Model A, Main Test Model.

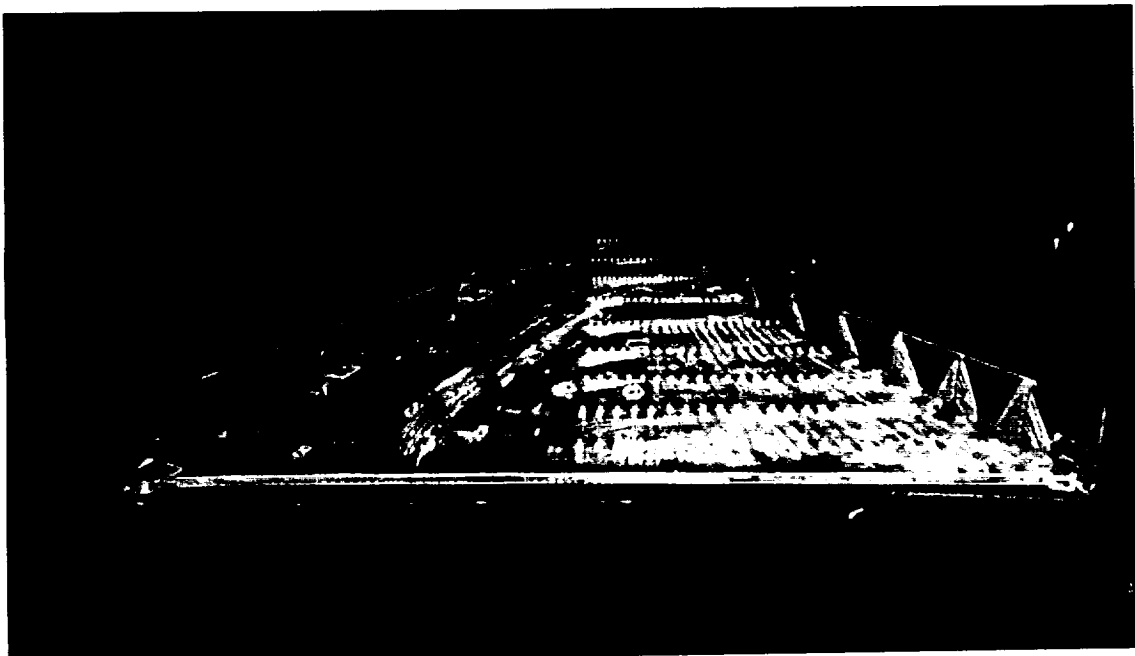
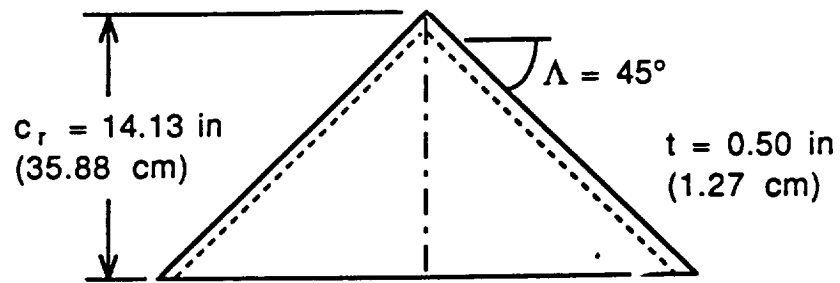
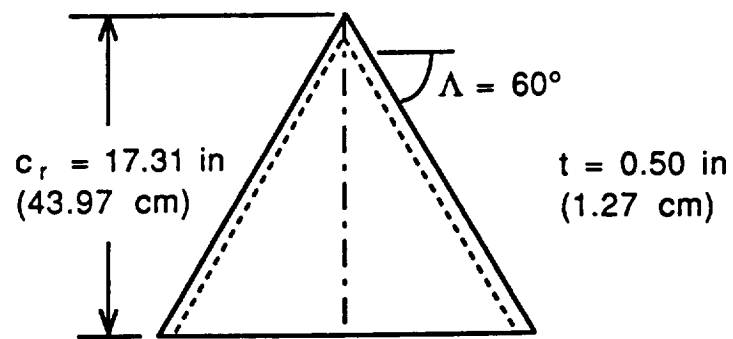


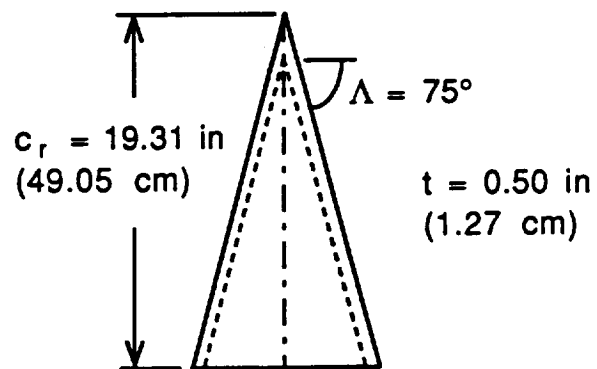
Figure 6. Model B, Surface Pressure Model.



Model C



Model D



Model E

Figure 7. Models with Varied Sweep Angle.

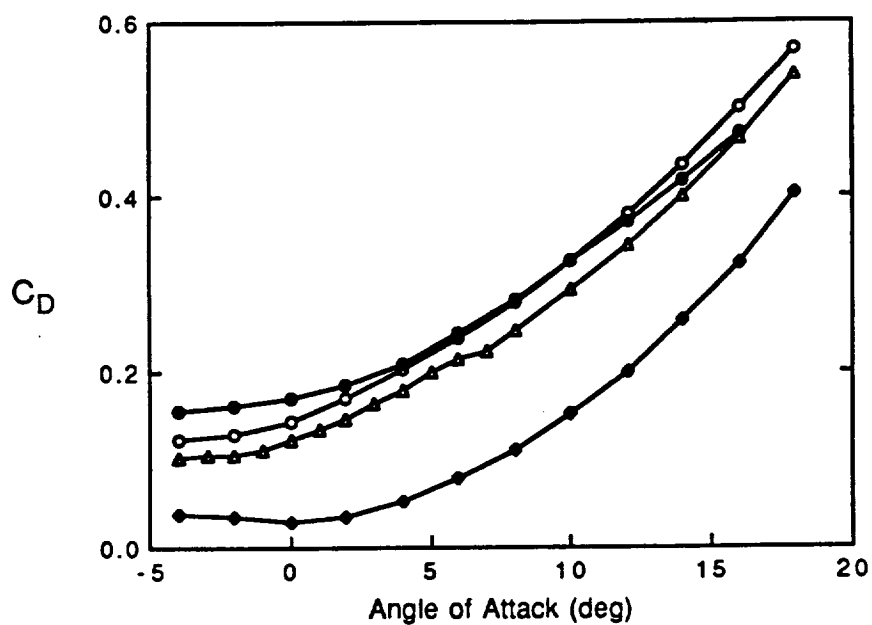
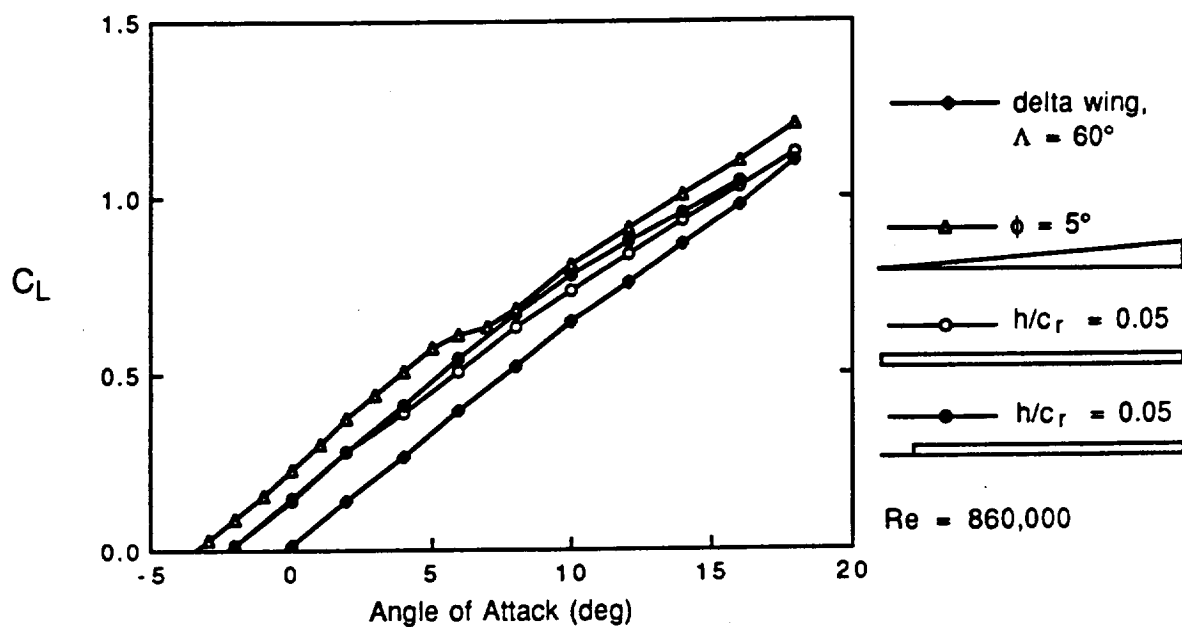


Figure 8. Effect of Fence Shape on Lift and Drag Coefficients.

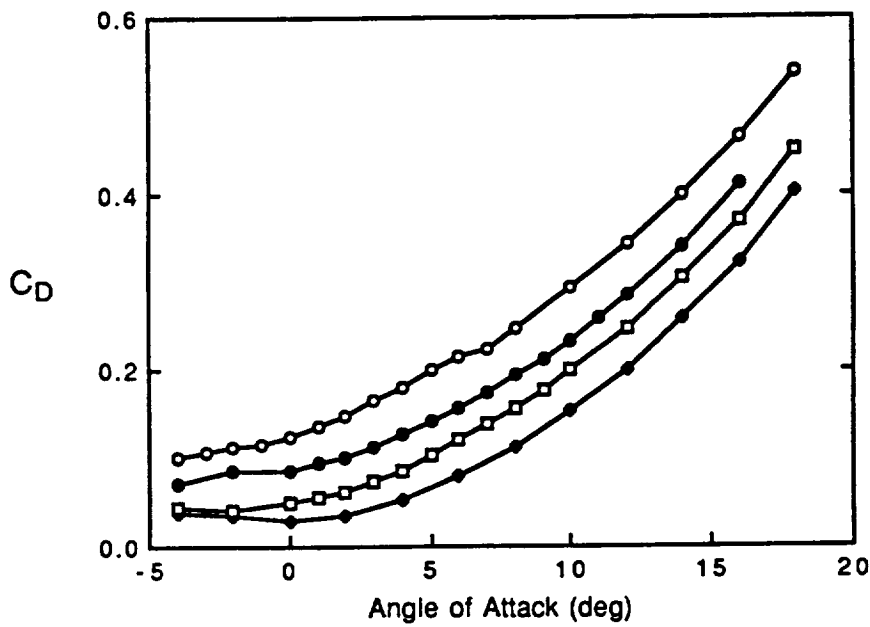
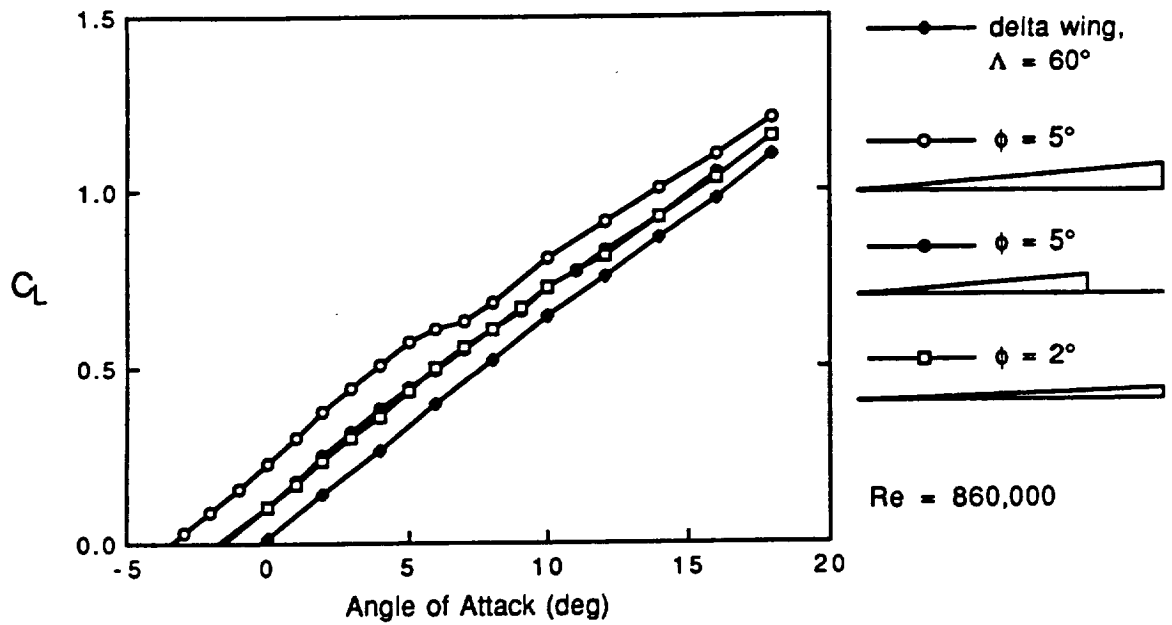


Figure 9. Effect of Fence Length on Lift and Drag Coefficients.

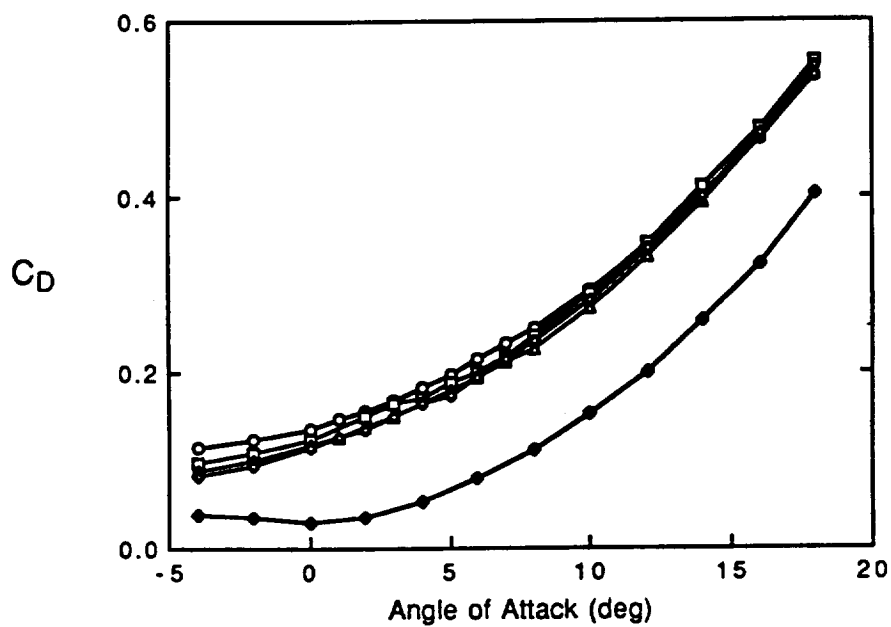
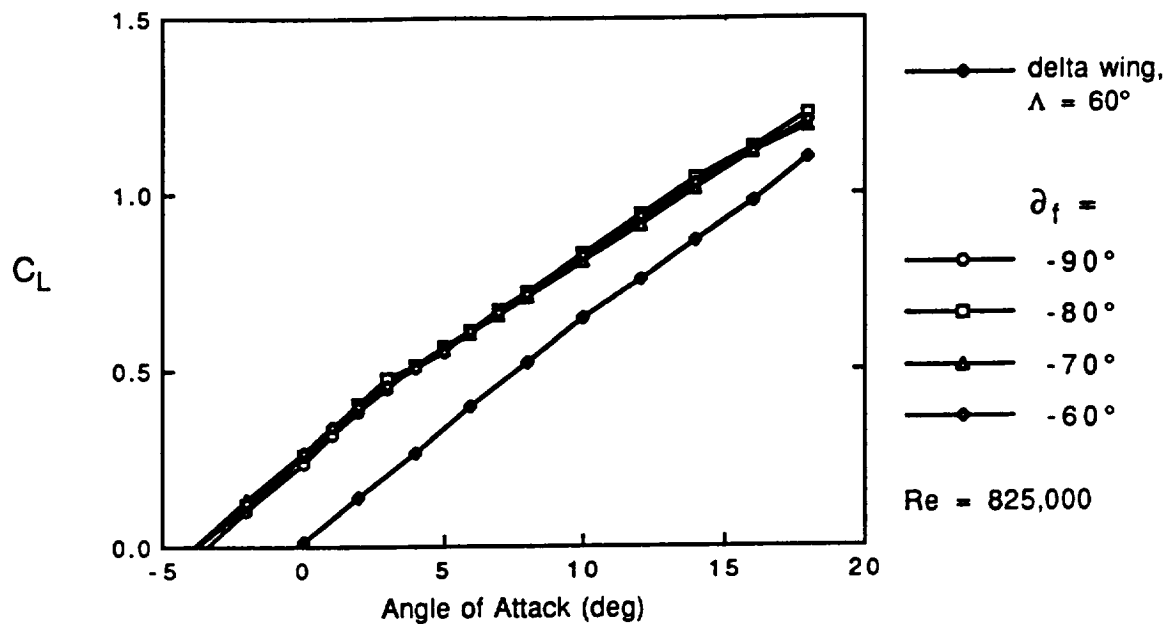


Figure 10. Effect of Deflection Angle on Lift and Drag Coefficients.

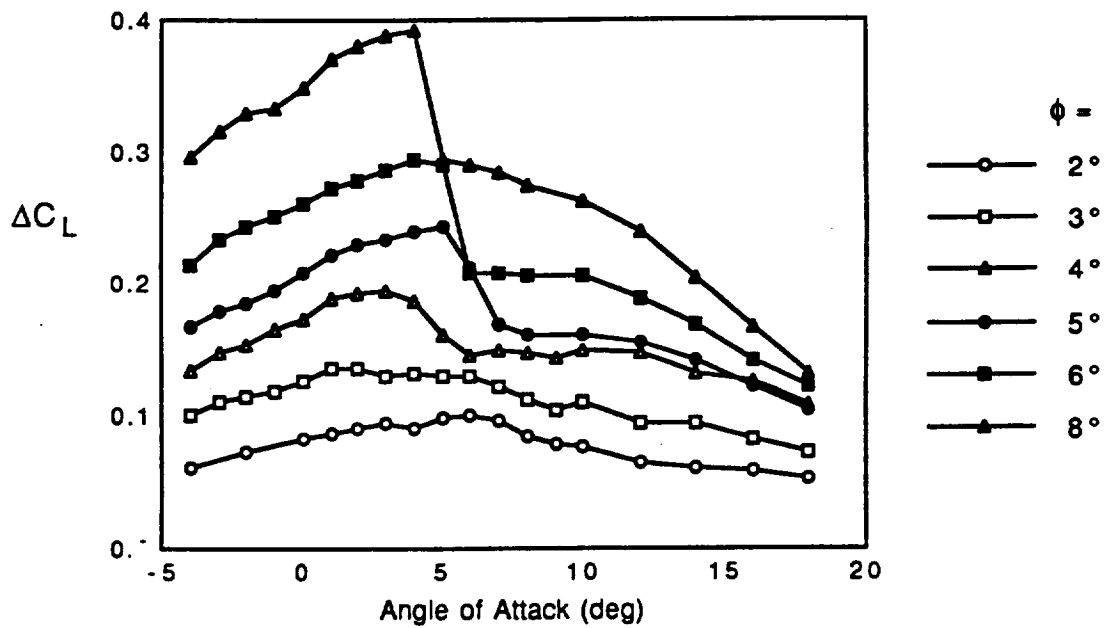
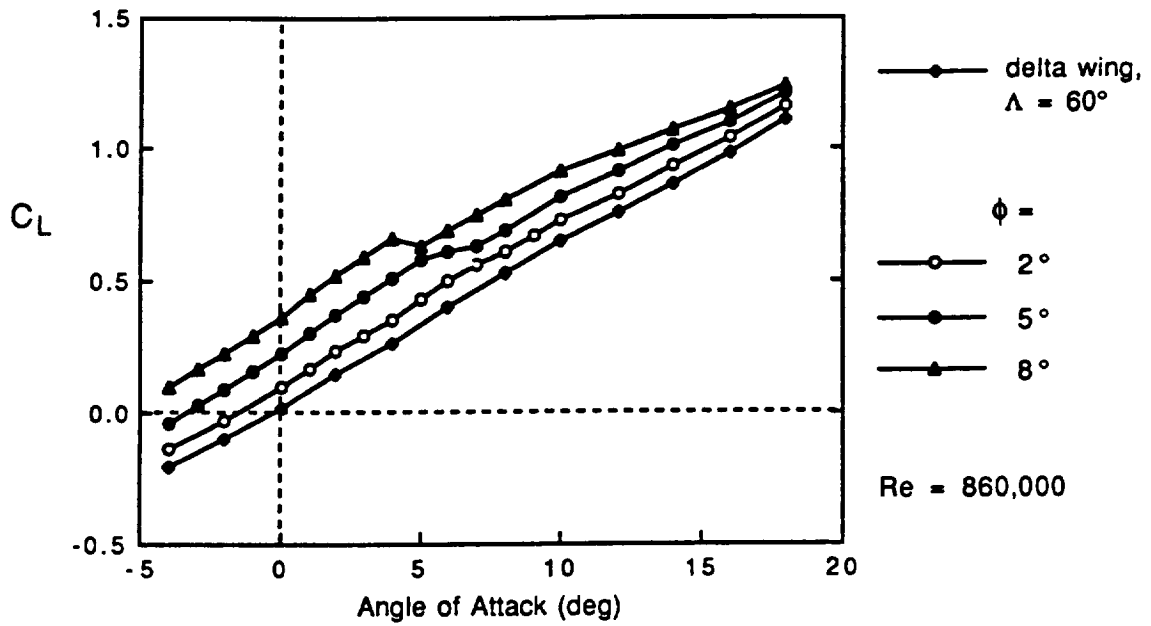


Figure 11. Effect of Fence Angle on Lift and Lift Gain.



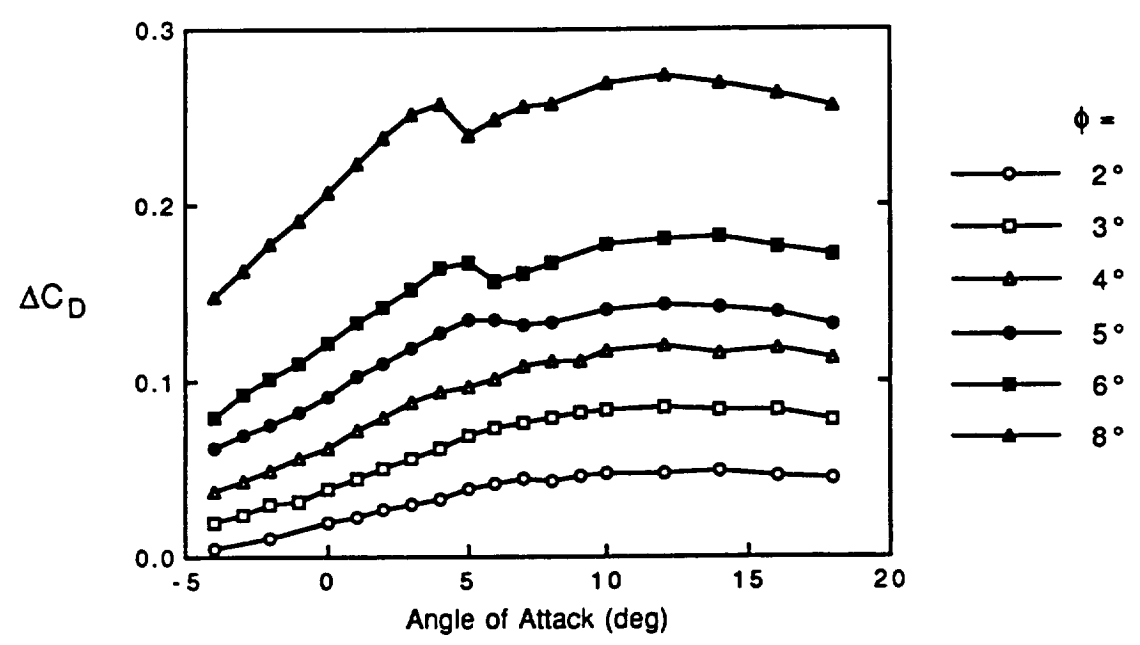
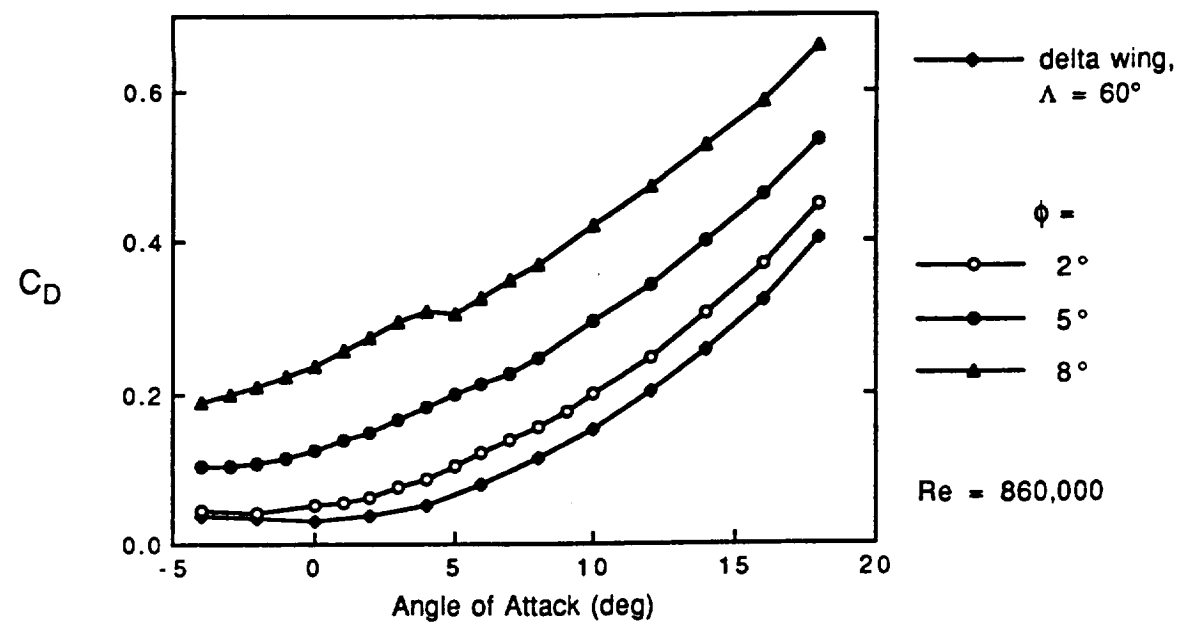


Figure 12. Effect of Fence Angle on Drag and Drag Gain.

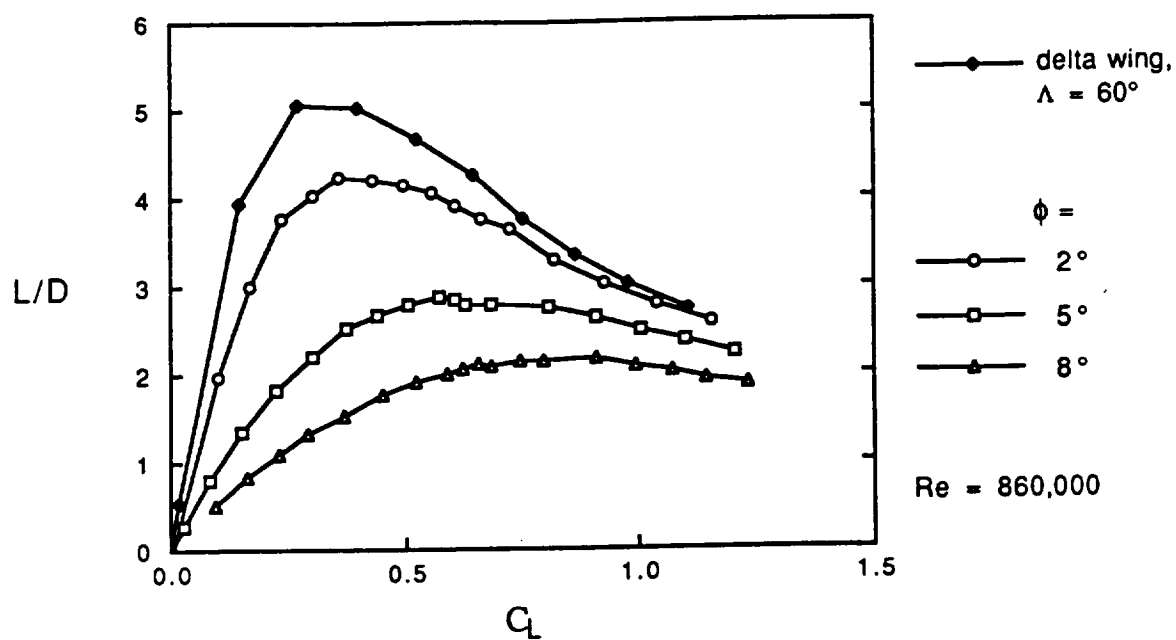


Figure 13. Effect of Fence Angle on Lift to Drag Ratio.

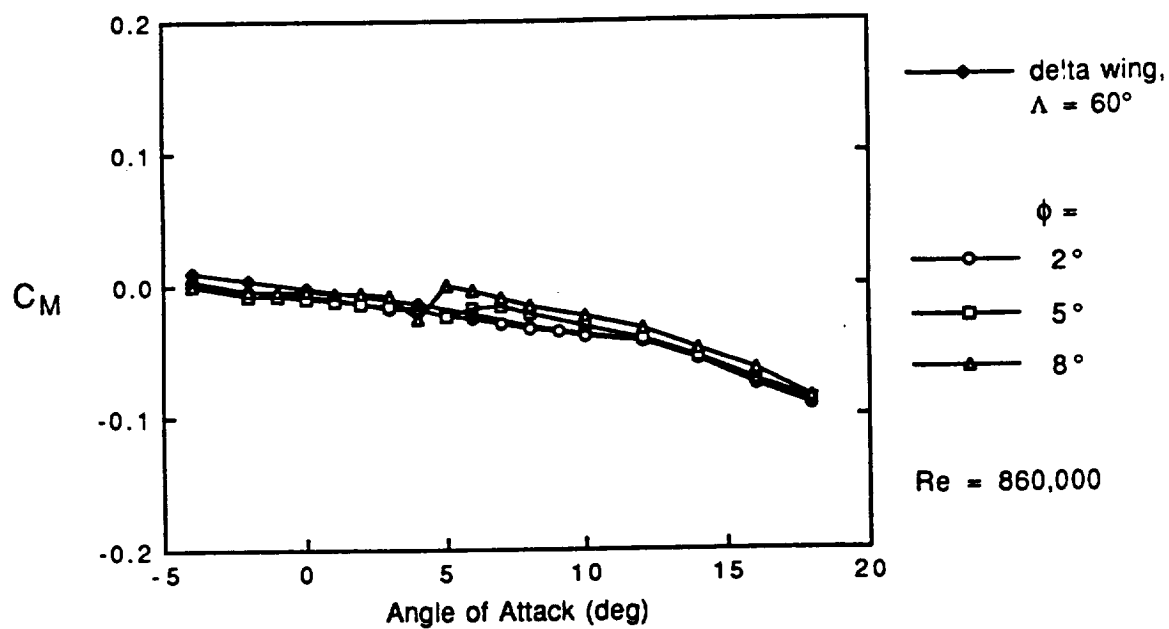


Figure 14. Effect of Fence Angle on Pitching Moment.

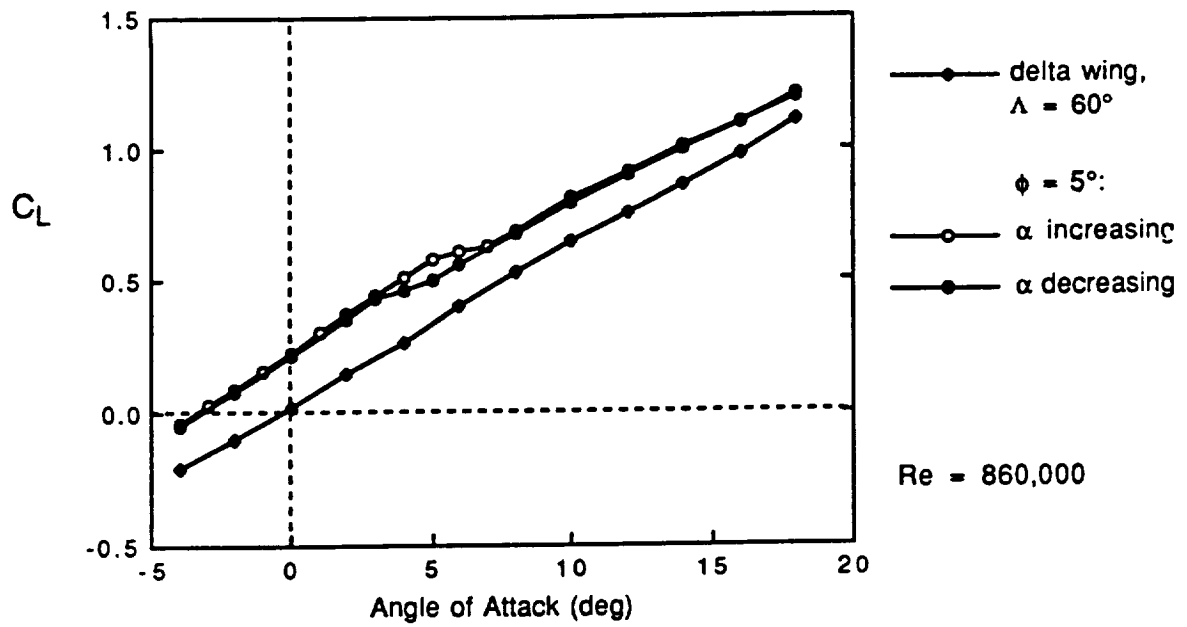


Figure 15. Hysteresis of the Lift Coefficient.

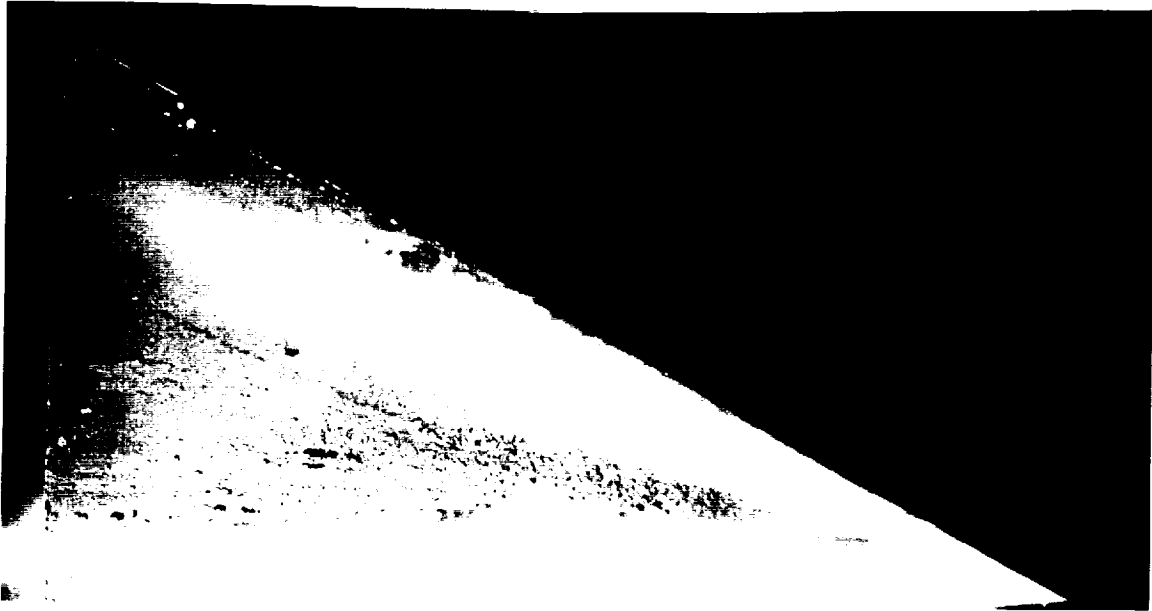


(a)  $\alpha = 0^\circ$



(b)  $\alpha = 3^\circ$

Figure 16. Vapor Patterns on 60° Delta Wing;  $Re = 430,000$ .



(c)  $\alpha = 6^\circ$



(d)  $\alpha = 10^\circ$

Figure 16. Continued.



(e)  $\alpha = 14^\circ$

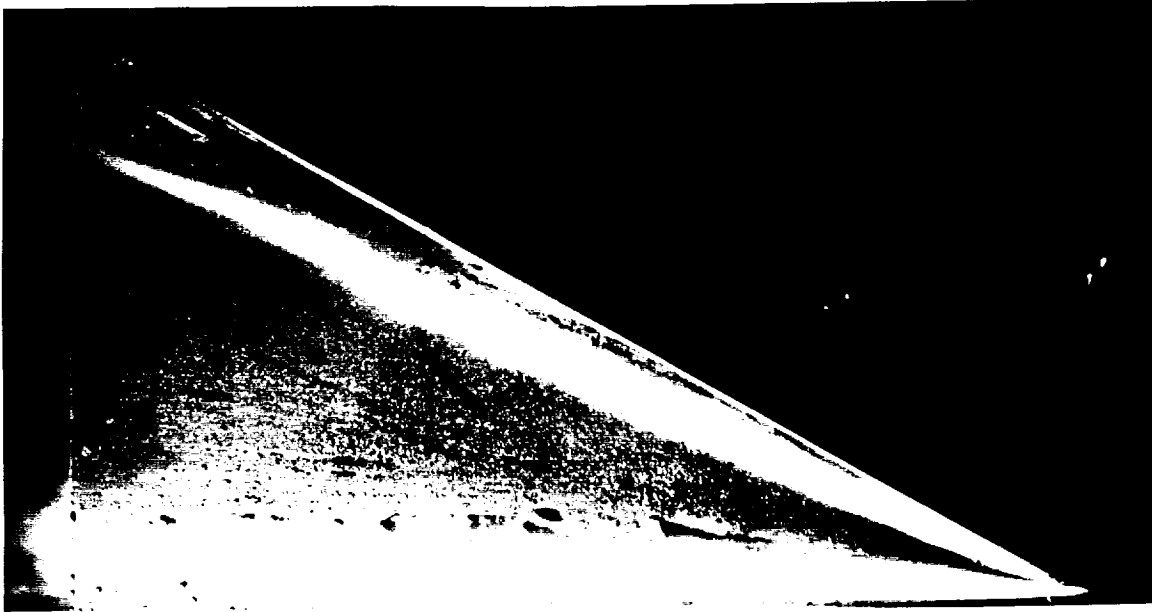


(f)  $\alpha = 20^\circ$

Figure 16. Continued.

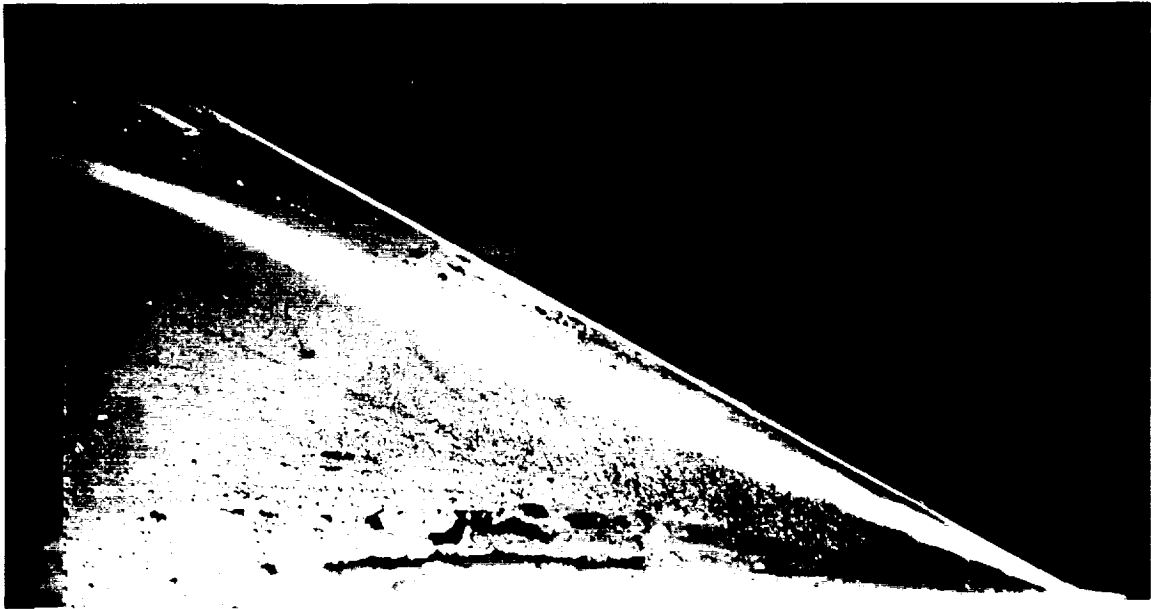


(a)  $\alpha = 0^\circ$

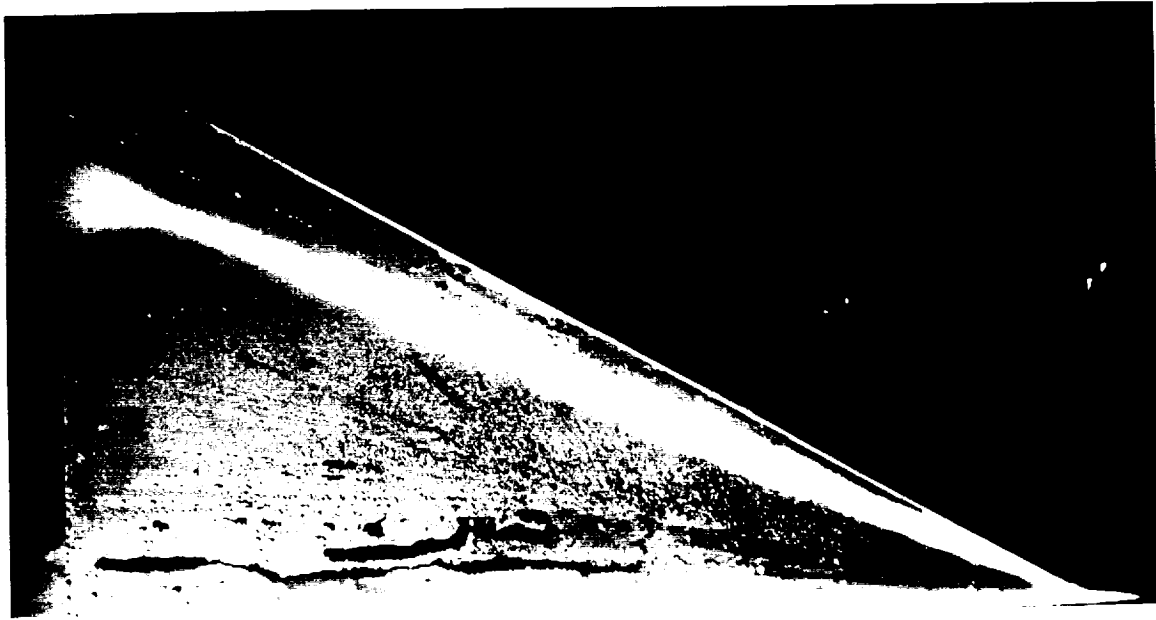


(b)  $\alpha = 3^\circ$

Figure 17. Vapor Patterns on  $60^\circ$  Delta Wing with  $\phi = 5^\circ$  Fences;  
 $Re = 430,000$ .



(c)  $\alpha = 6^\circ$



(d)  $\alpha = 6^\circ$ , Occasionally

Figure 17. Continued.





(e)  $\alpha = 10^\circ$

Figure 17. Continued.

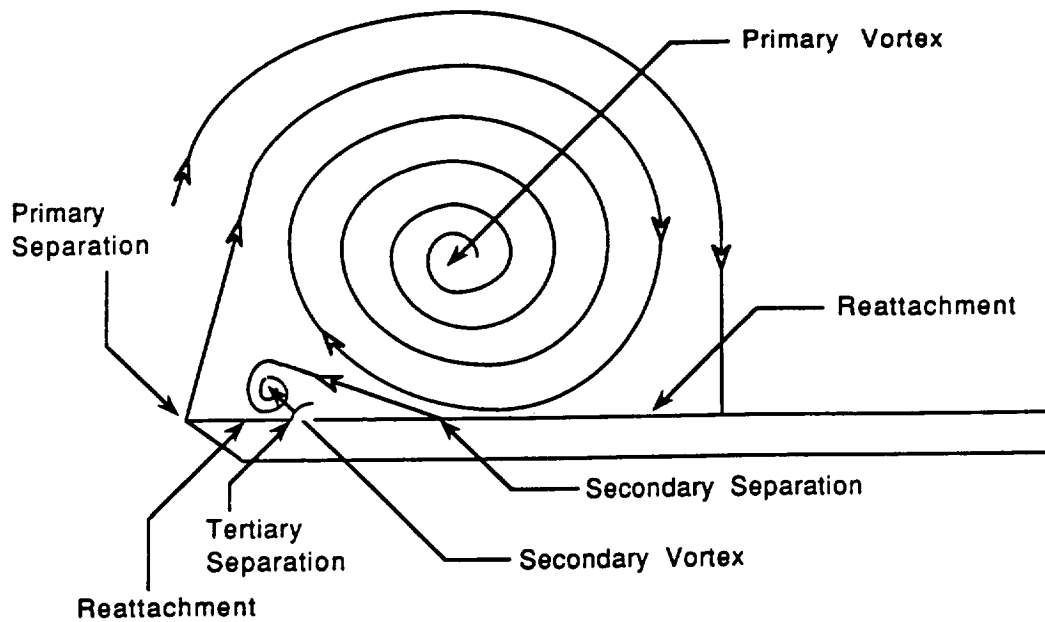
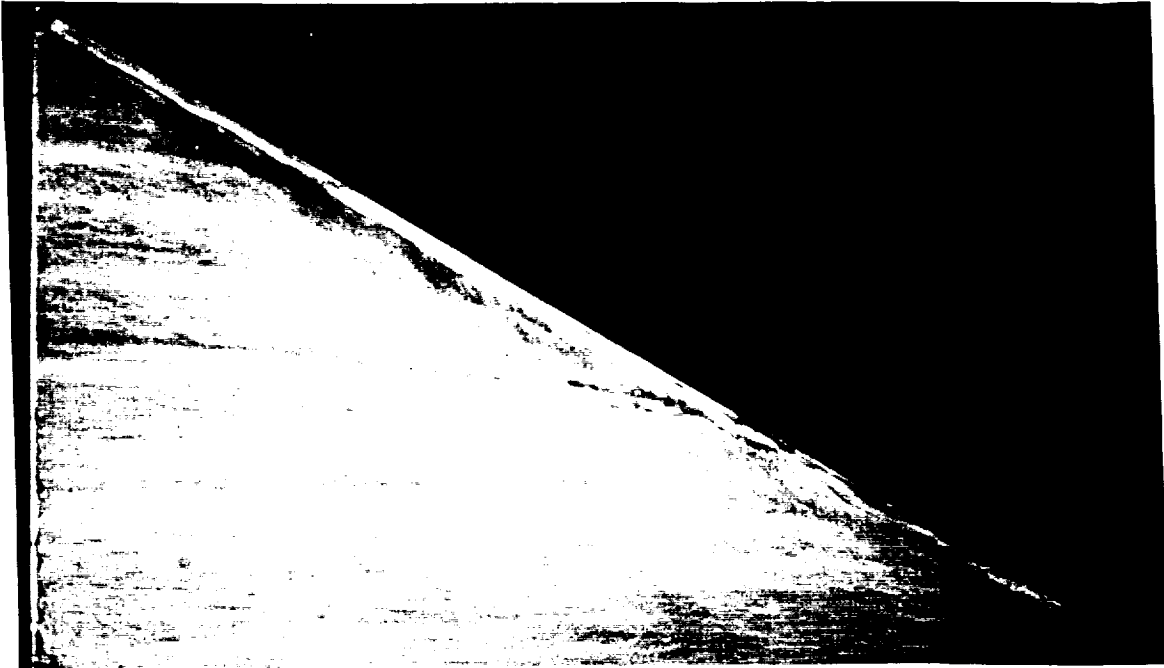
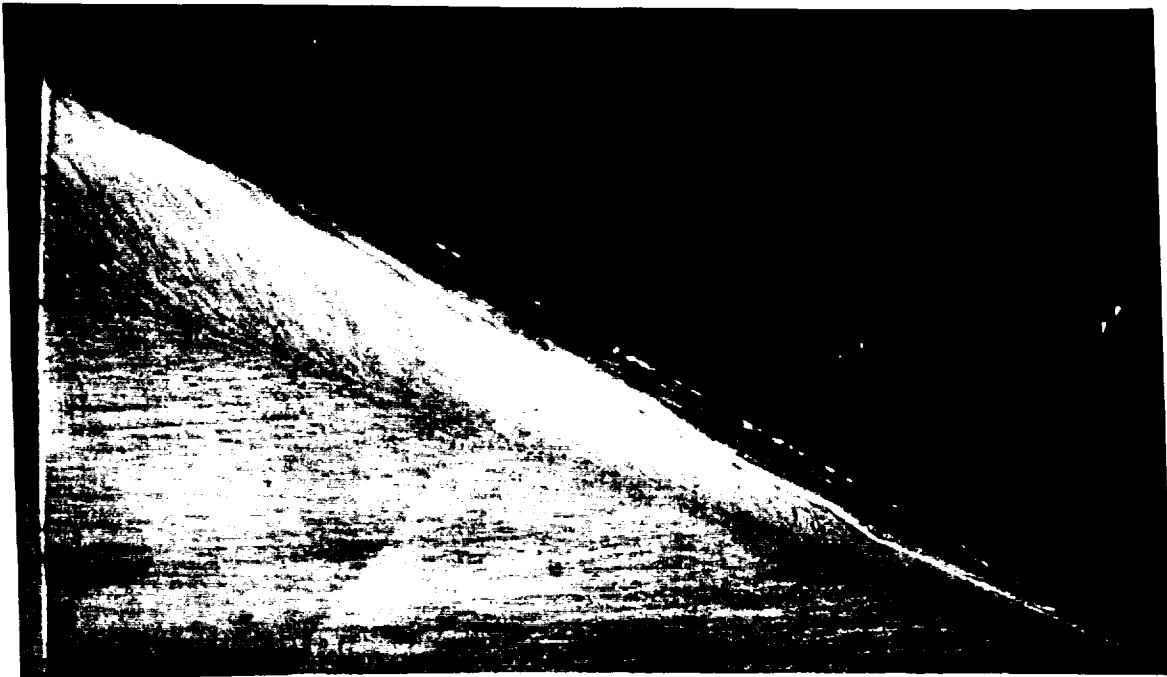


Figure 18. Typical Crossflow Patterns Above 60° Delta Wing;  
 $\alpha \approx 10^\circ$ .



(a)  $\alpha = 0^\circ$



(b)  $\alpha = 3^\circ$

Figure 19. Oil Patterns on 60° Delta Wing;  $Re = 600,000$ .

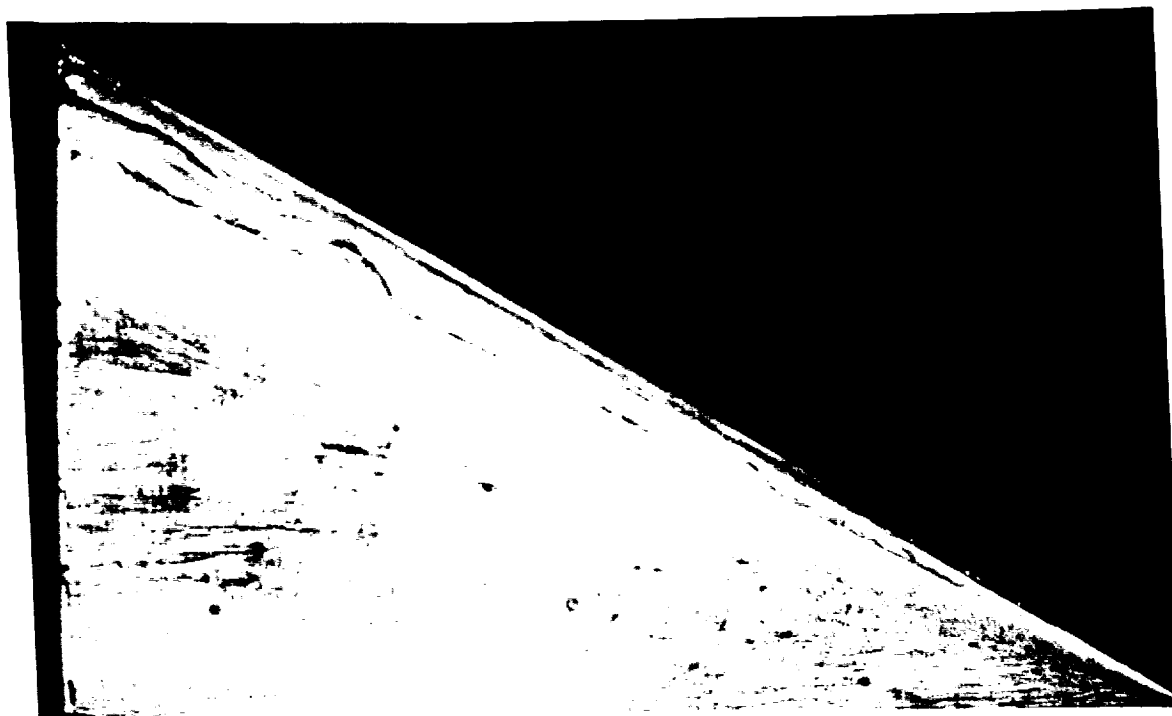


(c)  $\alpha = 6^\circ$



(d)  $\alpha = 10^\circ$

Figure 19. Continued.



(a)  $\alpha = 0^\circ$



(b)  $\alpha = 3^\circ$

Figure 20. Oil Patterns on 60° Delta Wing with  $\phi = 5^\circ$  Fences;  
Re = 600,000.



(c)  $\alpha = 6^\circ$



(d)  $\alpha = 10^\circ$

Figure 20. Continued.



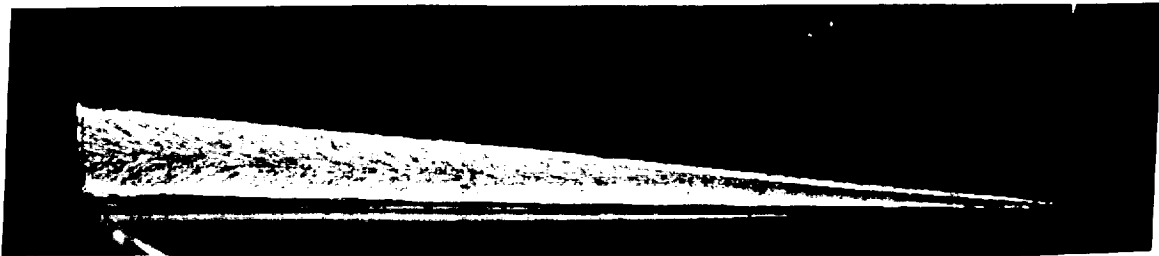
(a)  $\alpha = 0^\circ$ ; Outboard Side.



(b)  $\alpha = 0^\circ$ ; Inboard Side.



(c)  $\alpha = 10^\circ$ ; Outboard Side.



(d)  $\alpha = 10^\circ$ ; Inboard Side.

Figure 21. Oil Patterns on  $\phi = 5^\circ$  Fence;  $Re=600,000$ .

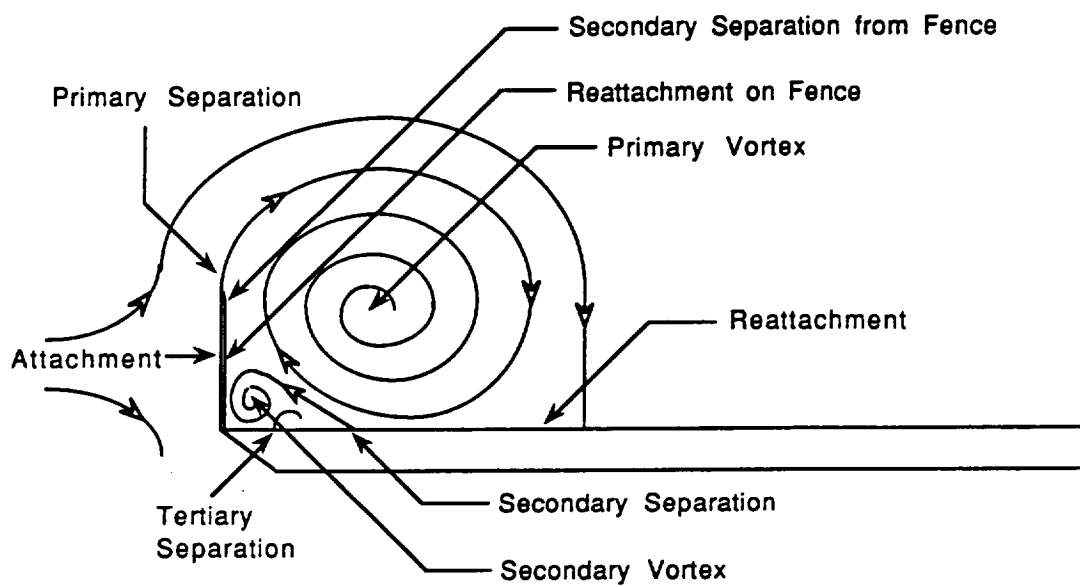


Figure 22. Typical Crossflow Patterns Above 60° Delta Wing with Fences;  $\alpha \approx 0^\circ$ . (Derived from Oil and Vapor Patterns).



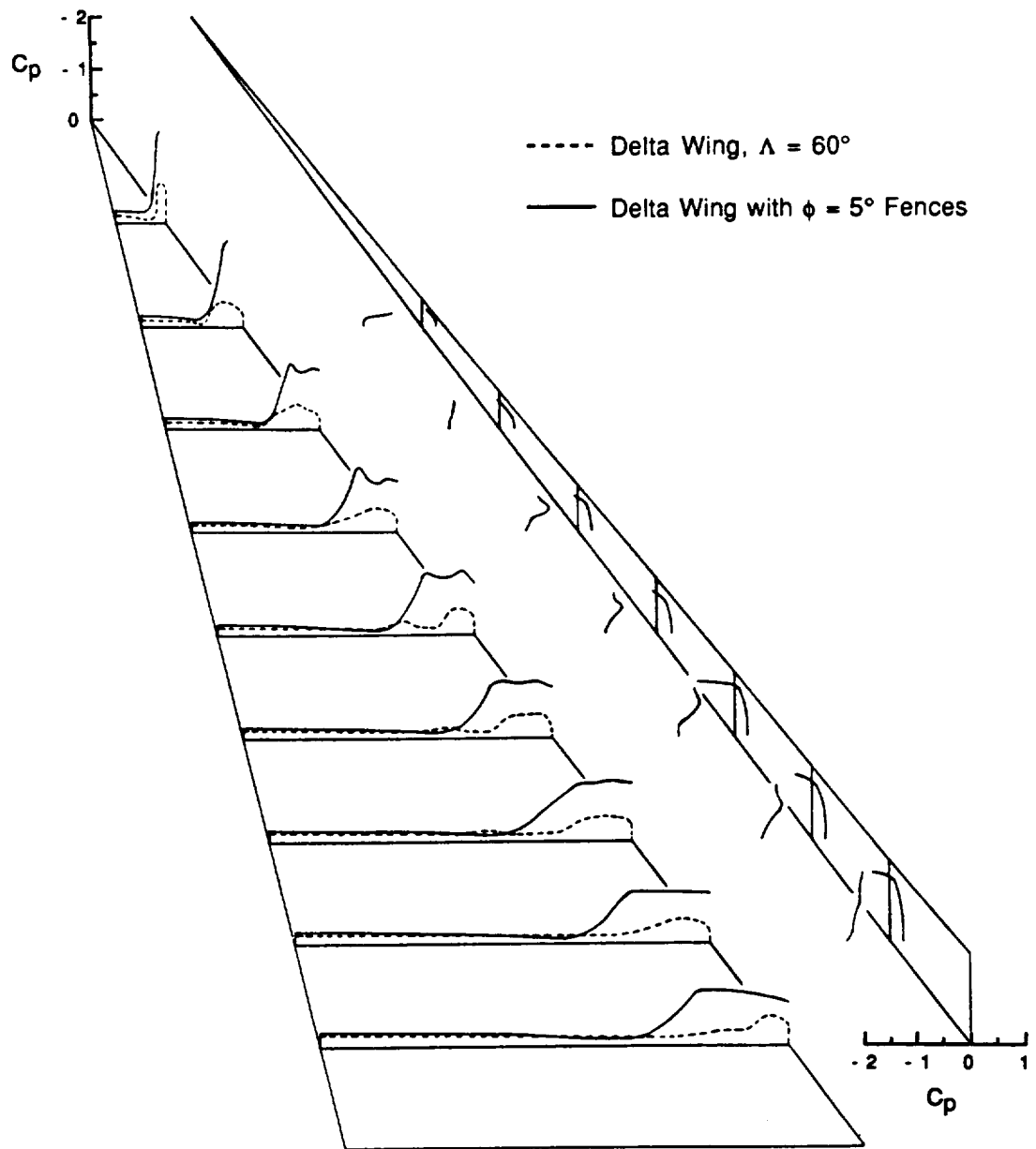
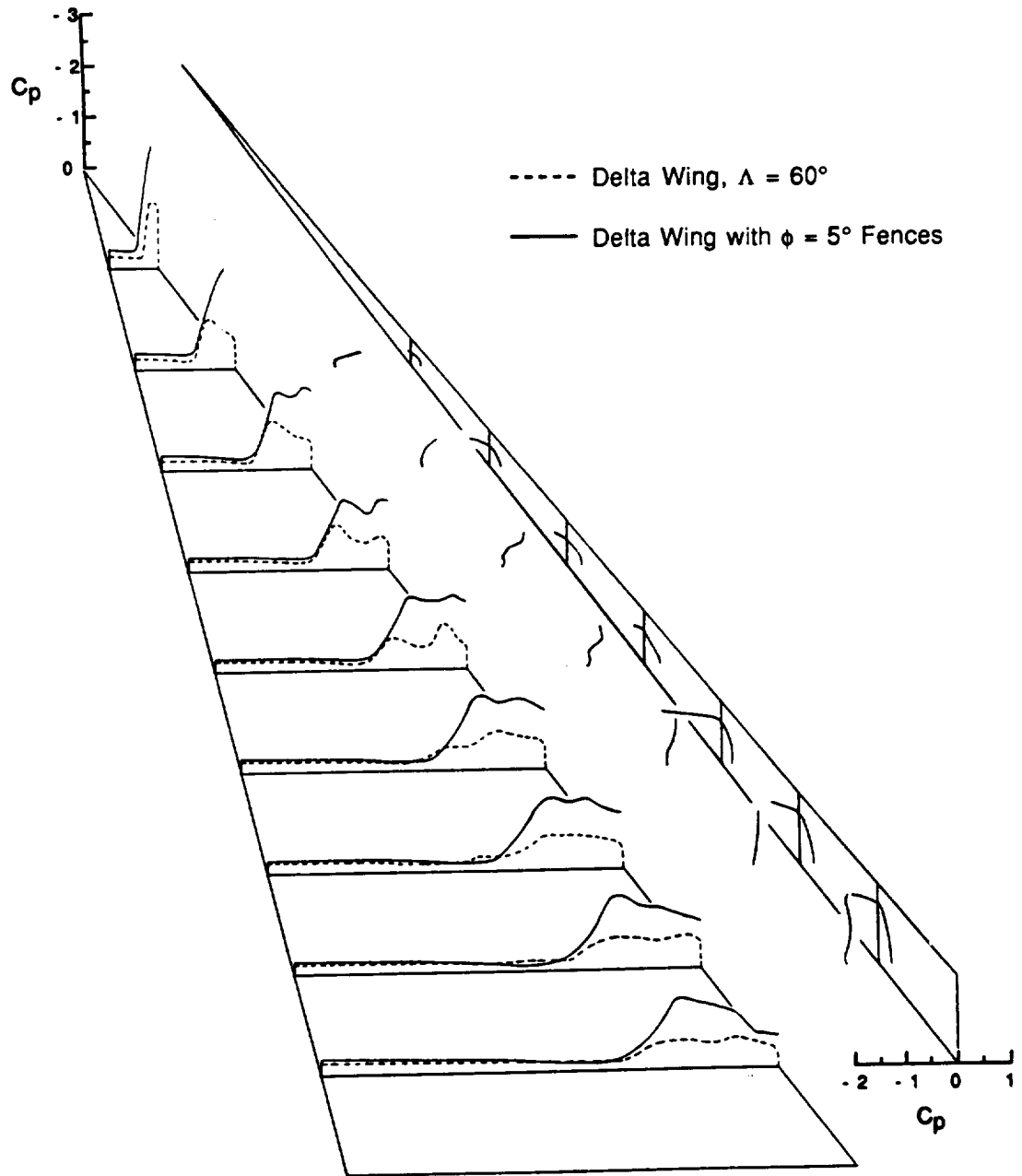
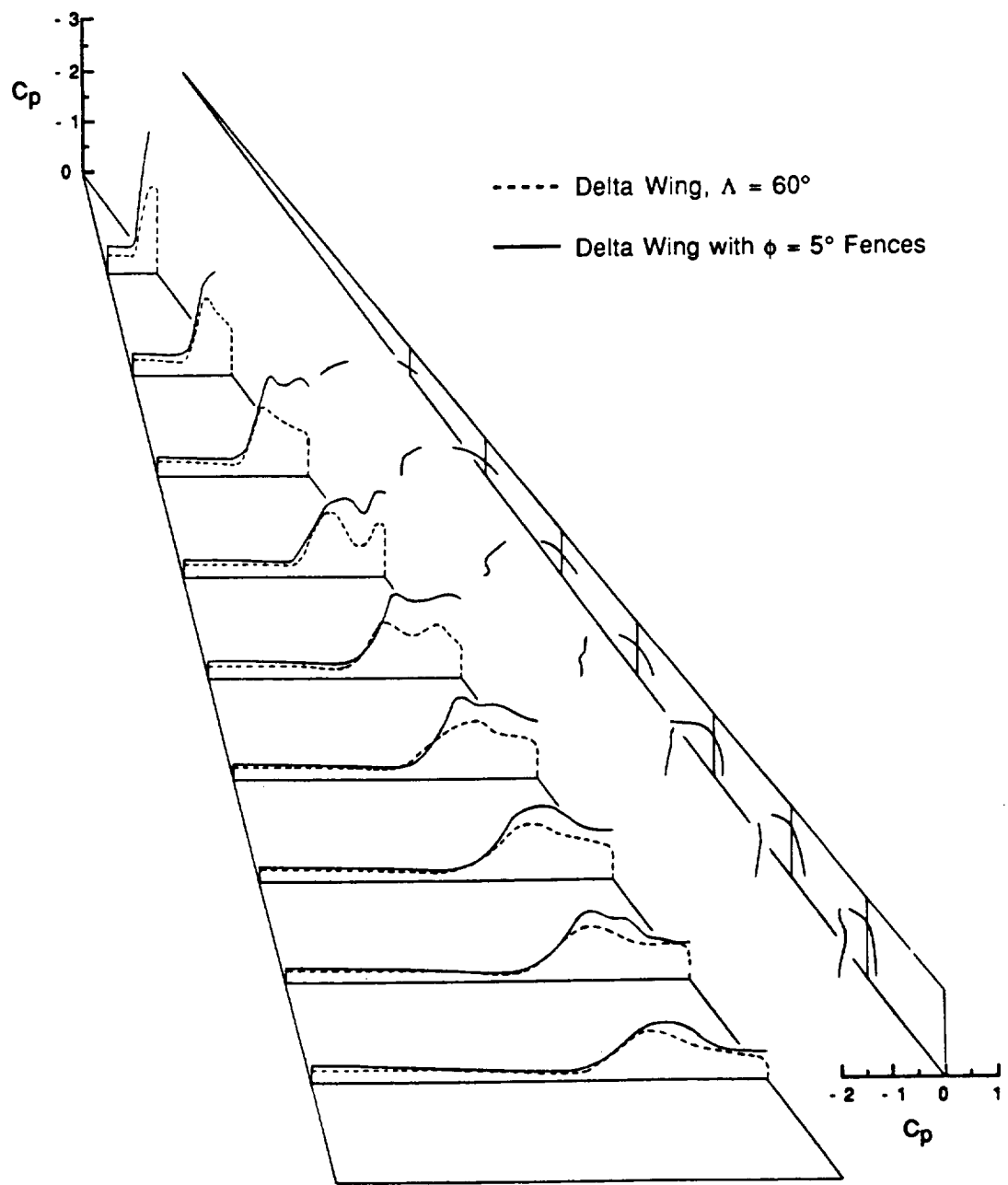


Figure 23. Surface Pressure Distributions;  $Re = 790,000$ .



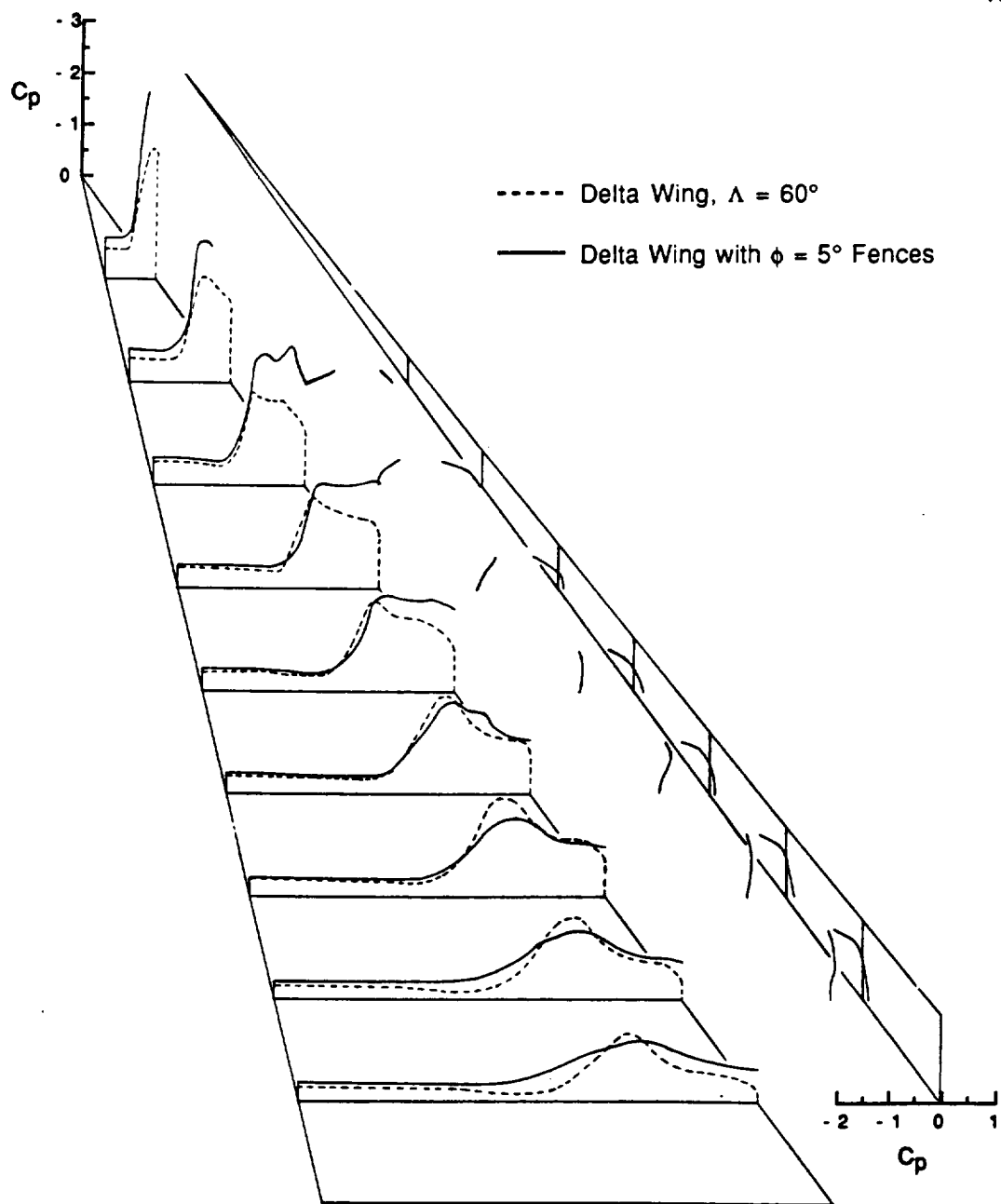
(b)  $\alpha = 3^\circ$

Figure 23. Continued.



(c)  $\alpha = 6^\circ$

Figure 23. Continued.



(d)  $\alpha = 10^\circ$

Figure 23. Continued.

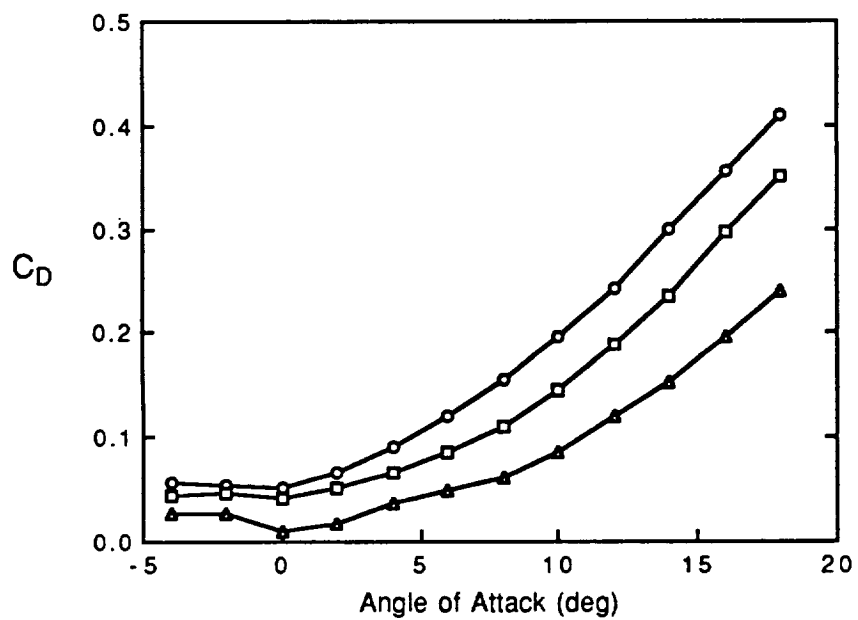
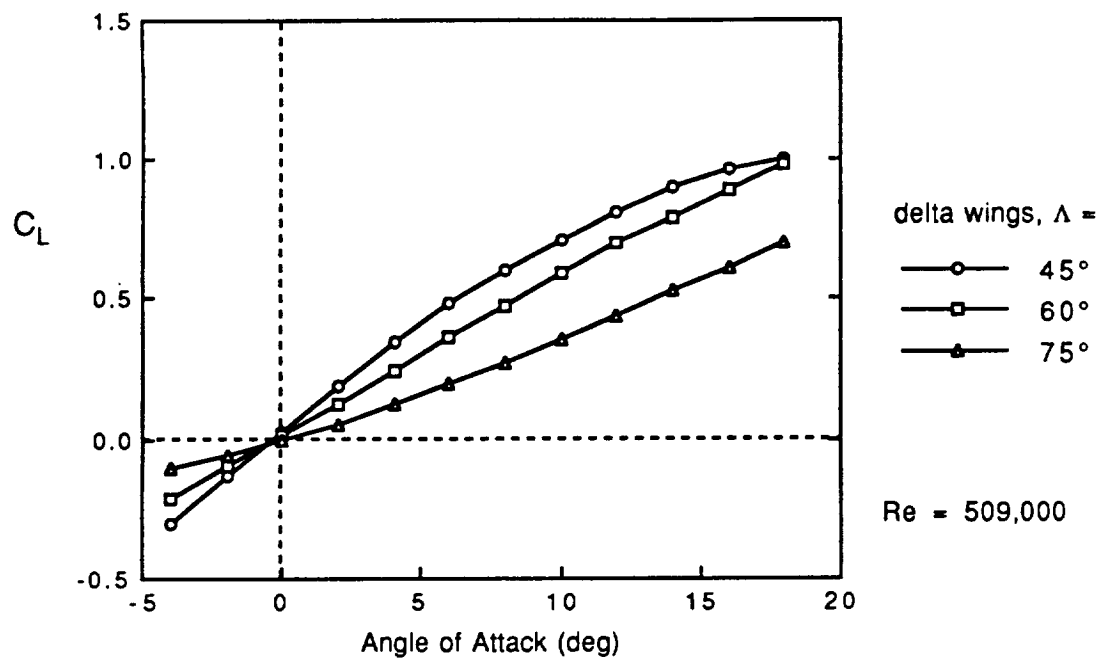


Figure 24. Lift and Drag of Delta Wings of Various Sweep Angle.

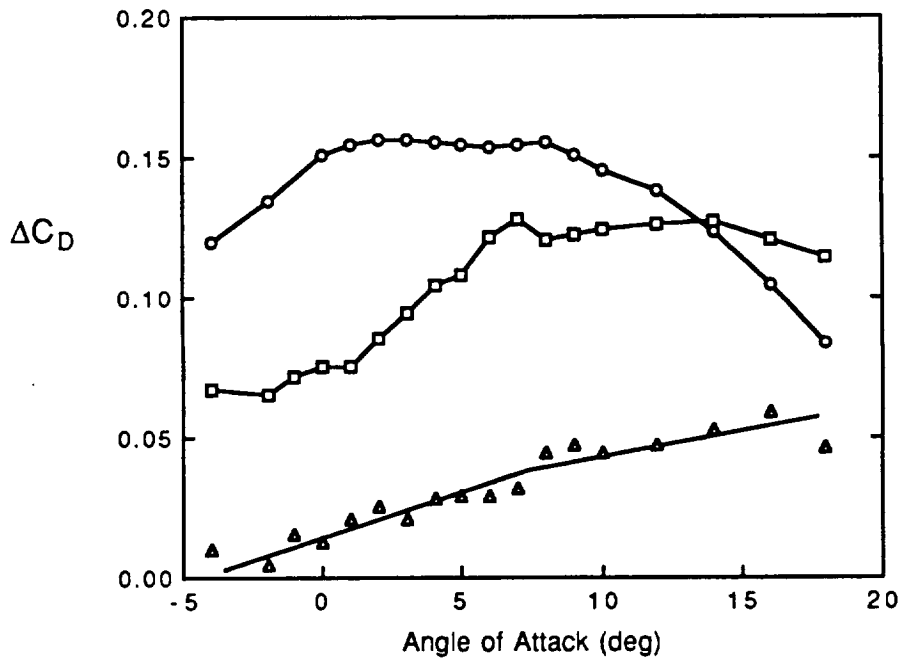
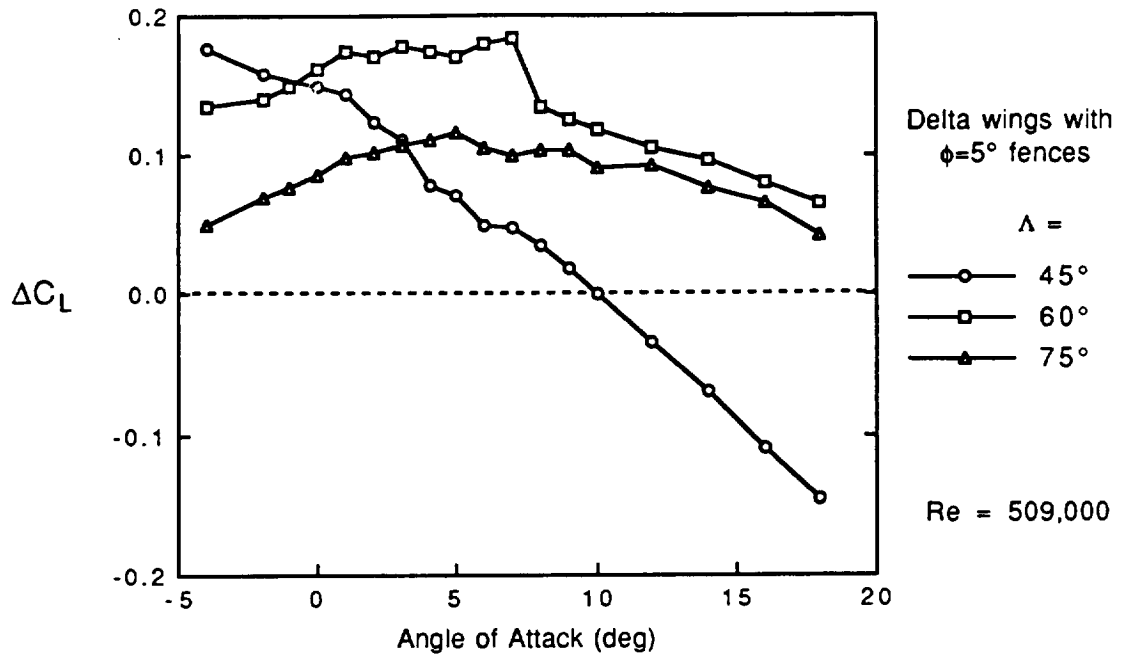


Figure 25. Gain in Lift and Drag with Fences on Delta Wings of Various Sweep Angle.

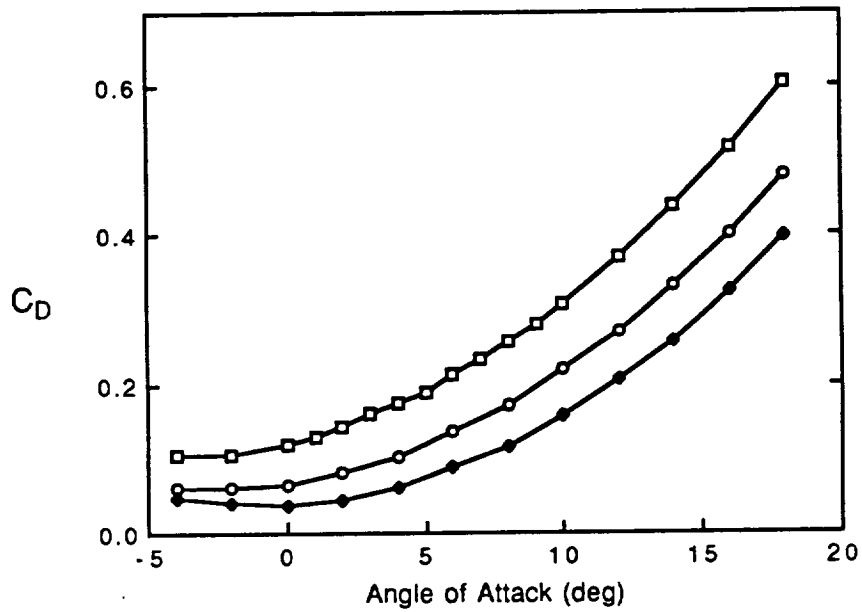
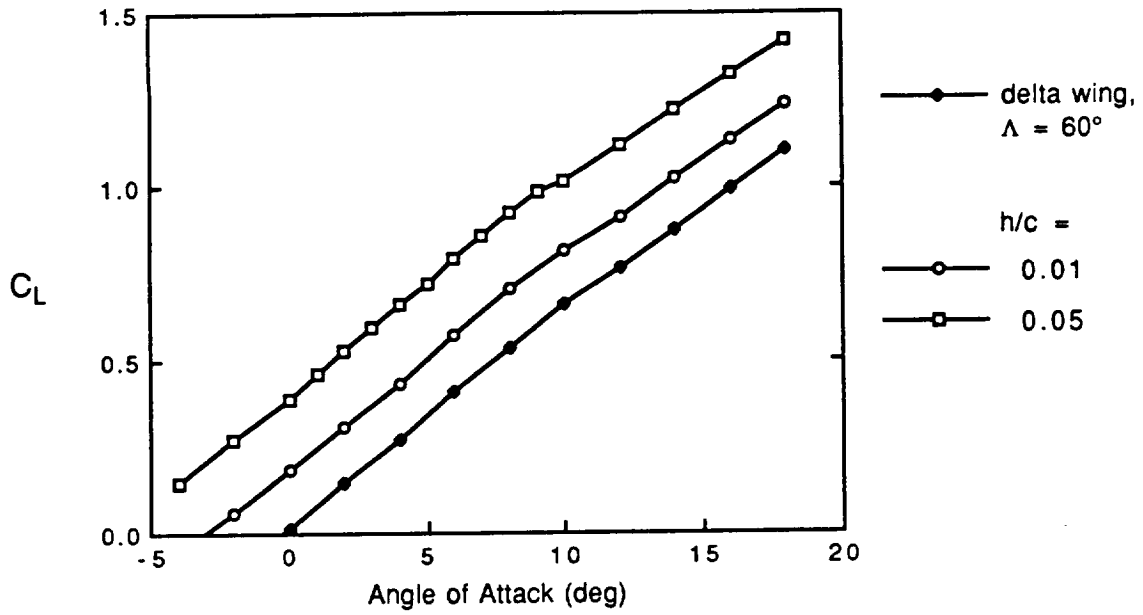


Figure 26. Lift and Drag for Tapered Height Gurney Flap.

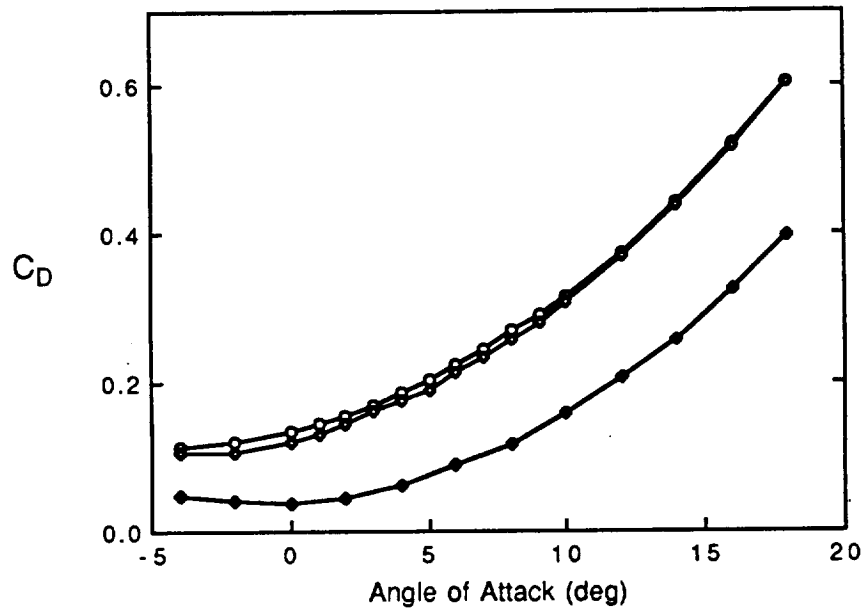
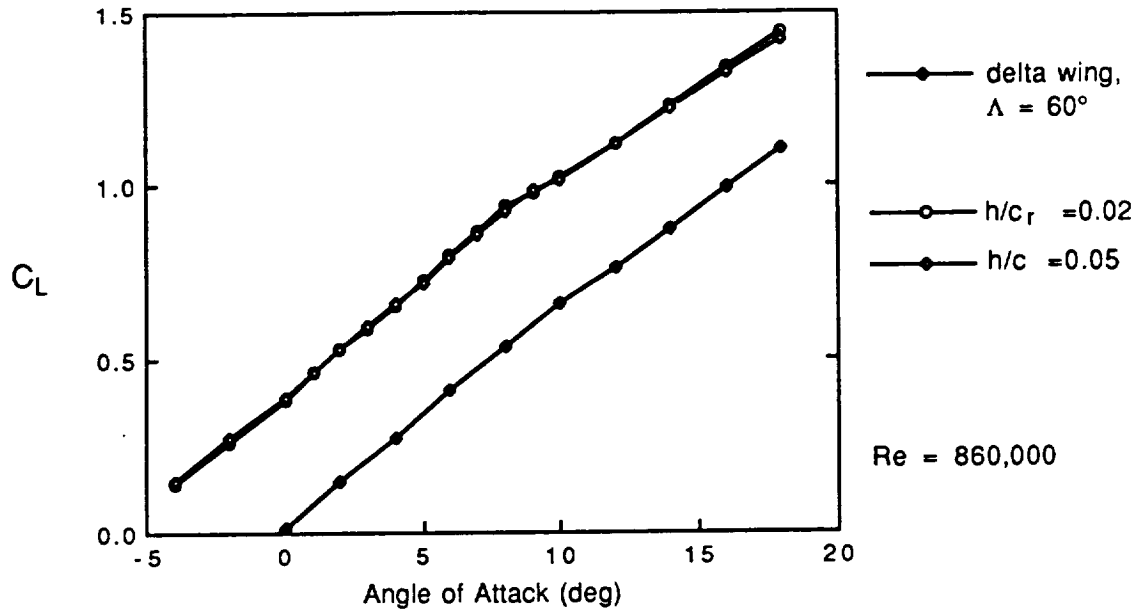


Figure 27. Lift and Drag Comparison of Constant Height and Tapered Height Gurney Flaps.



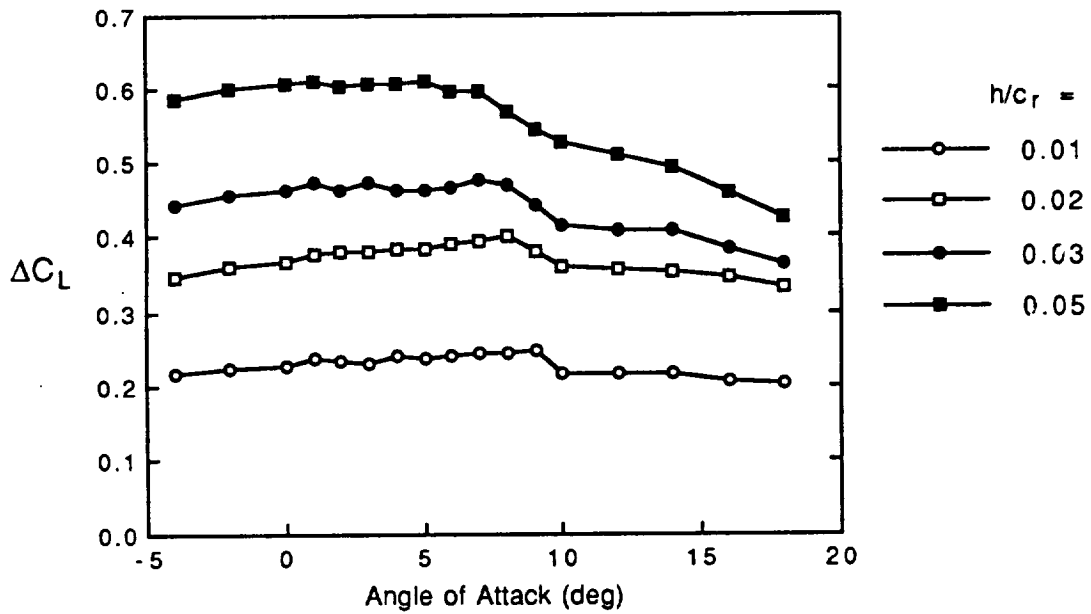
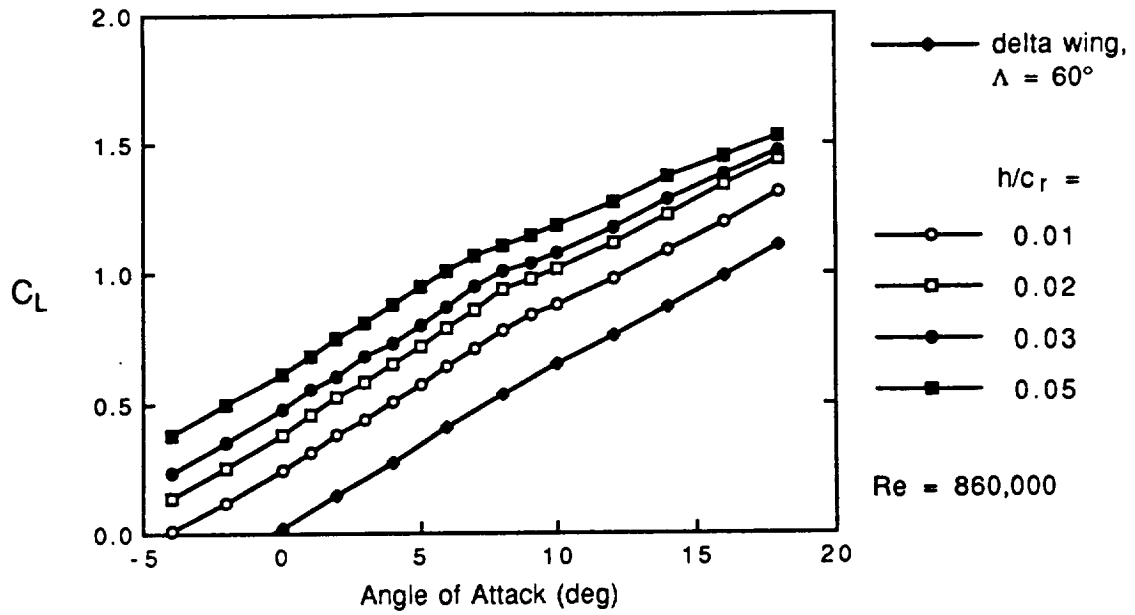


Figure 28. Lift and Lift Gain for Constant Height Gurney Flap.

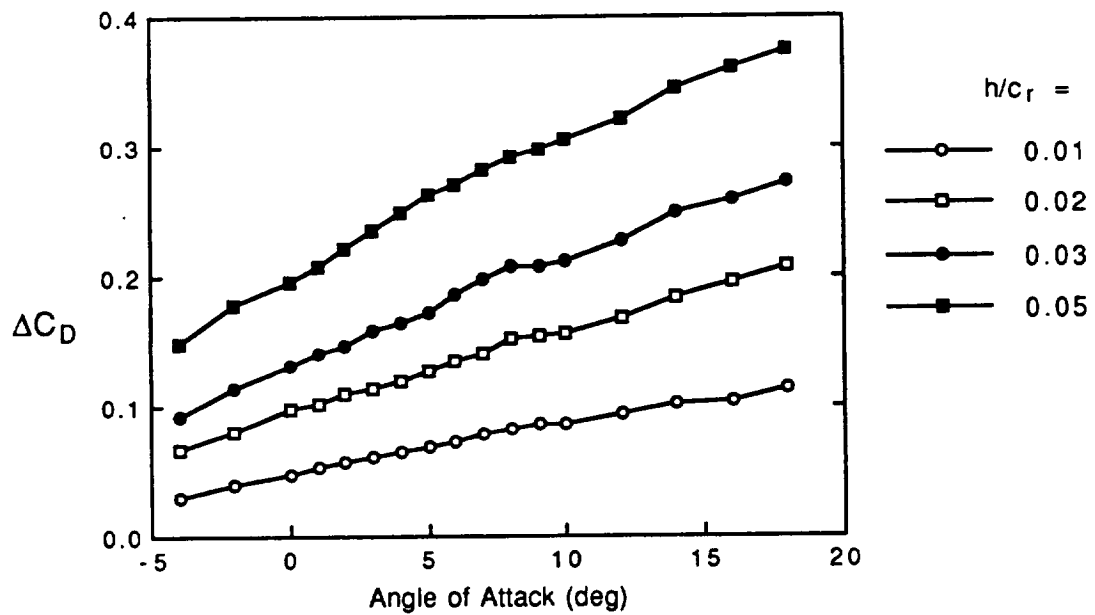
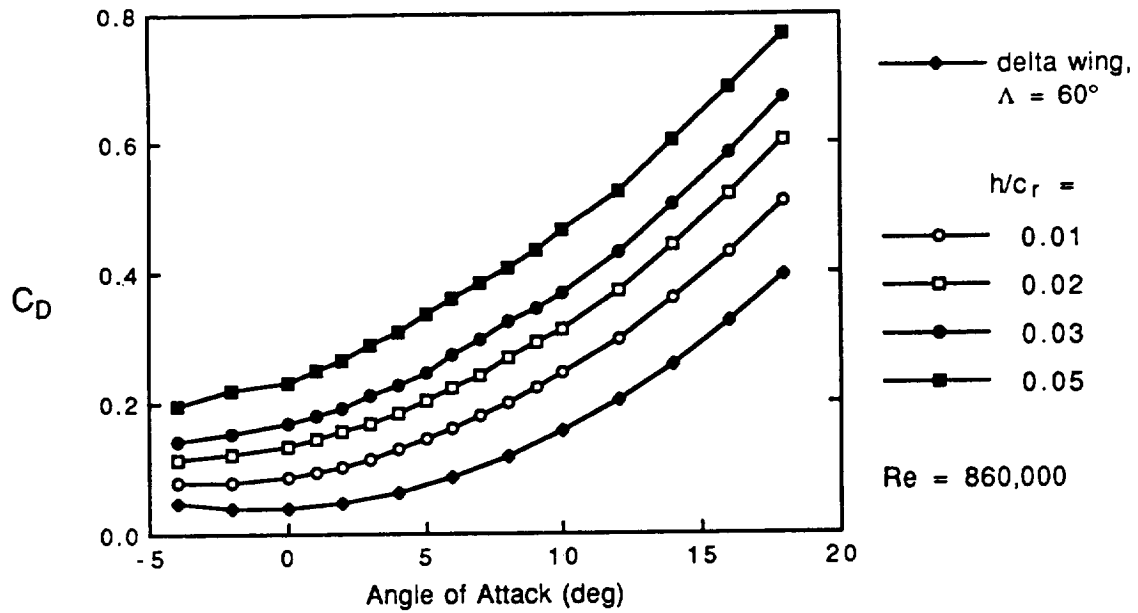


Figure 29. Drag and Drag Gain for Constant Height Gurney Flap.

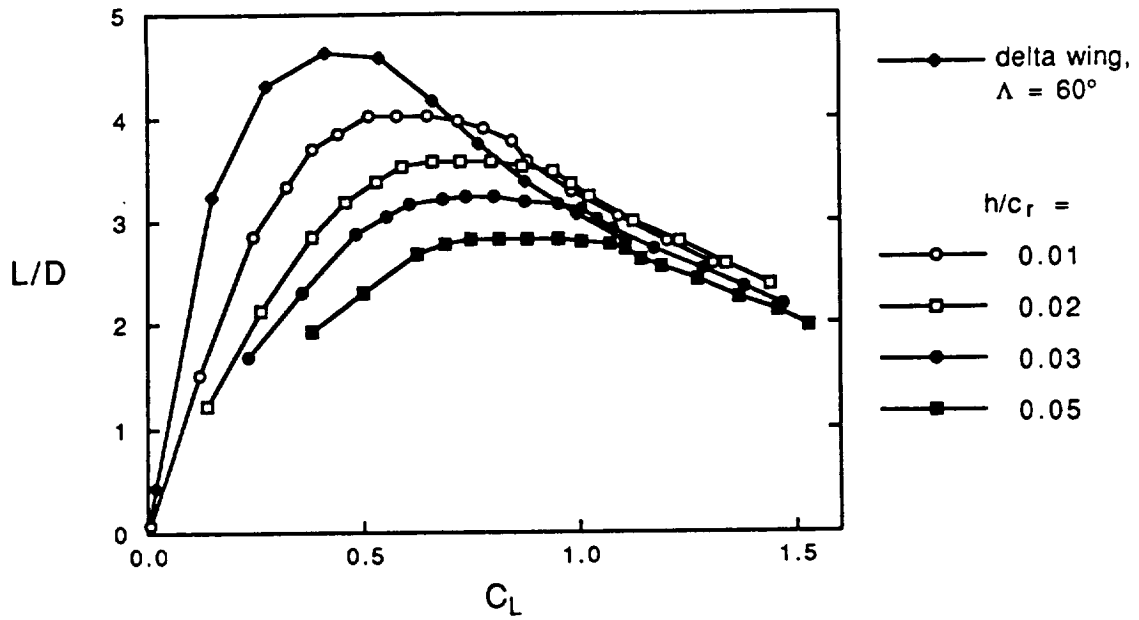


Figure 30.  $L/D$  for Constant Height Gurney Flap.

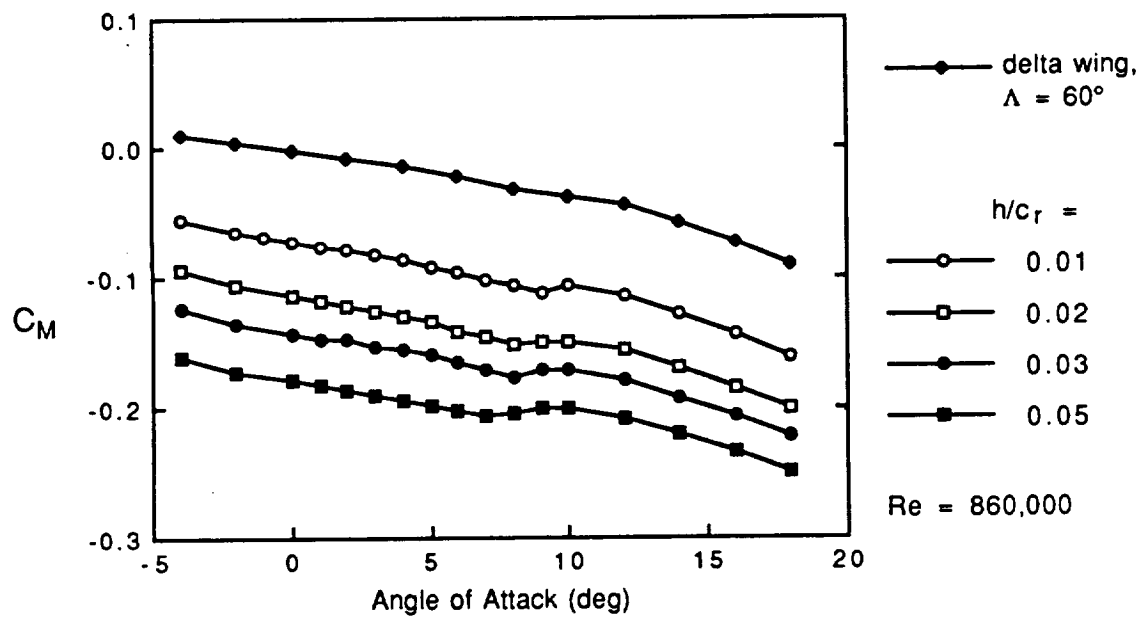
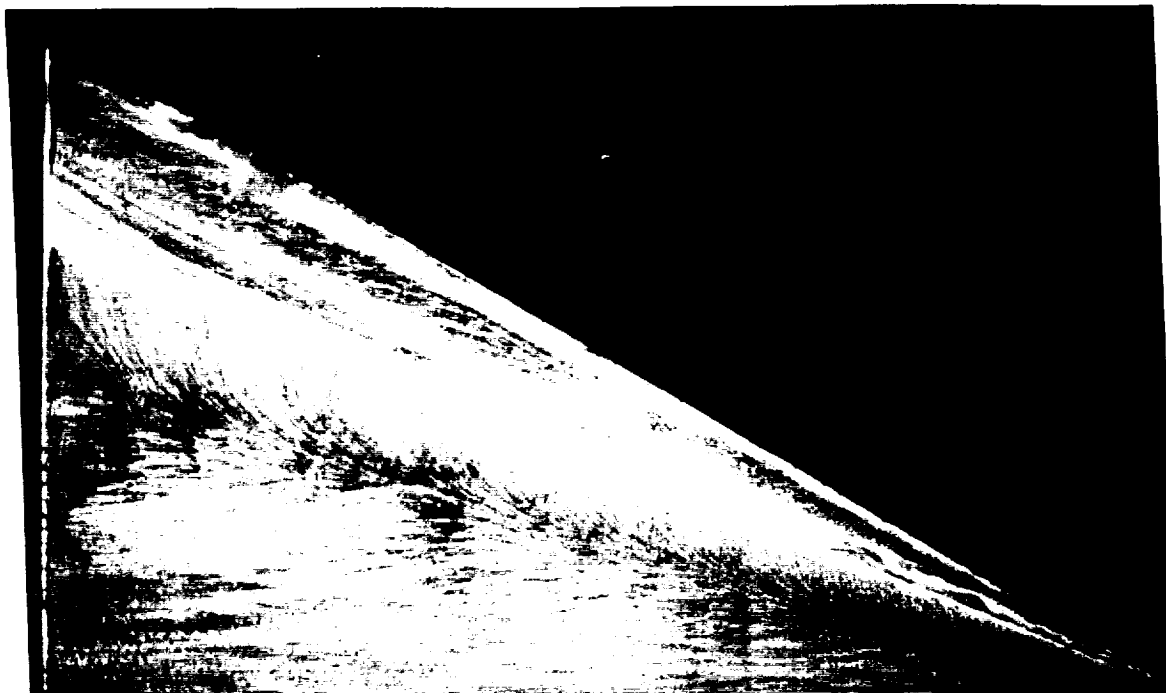
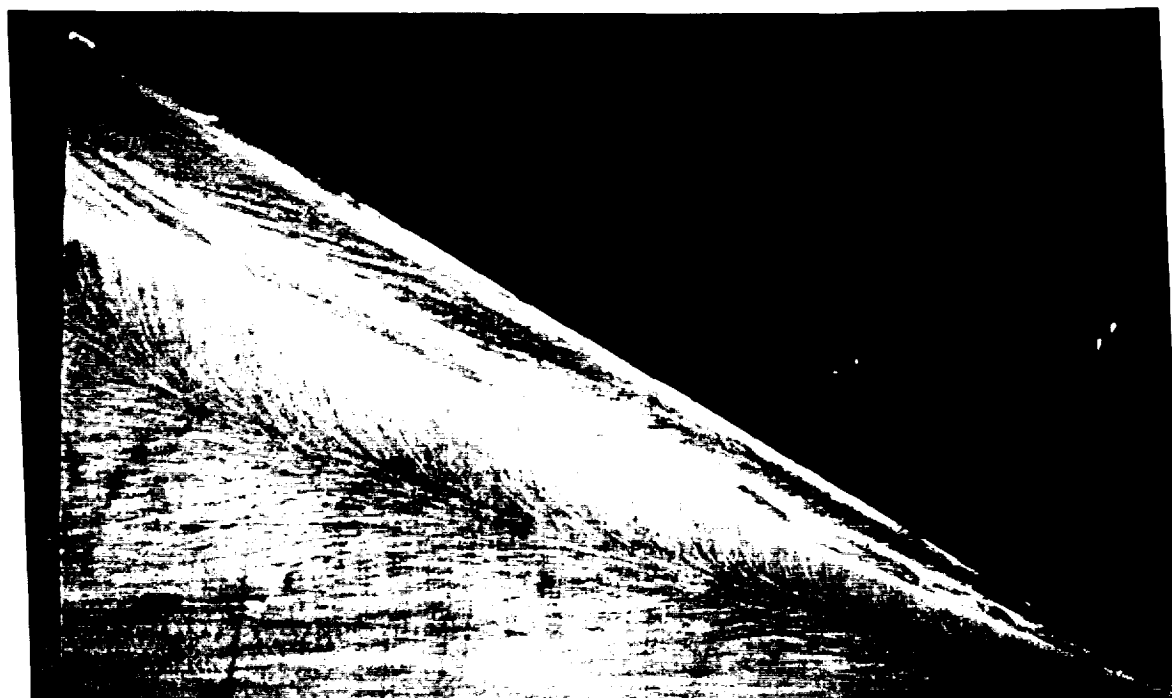


Figure 31. Pitching Moment for Constant Height Gurney Flap.



(a)  $\alpha = 10^\circ$ ; No Flap.



(b)  $\alpha = 10^\circ$ ; Flap  $h/c_r = 0.02$

Figure 32. Effect of Gurney Flap on Oil Patterns on 60° Delta Wing;  $Re = 600,000$ .

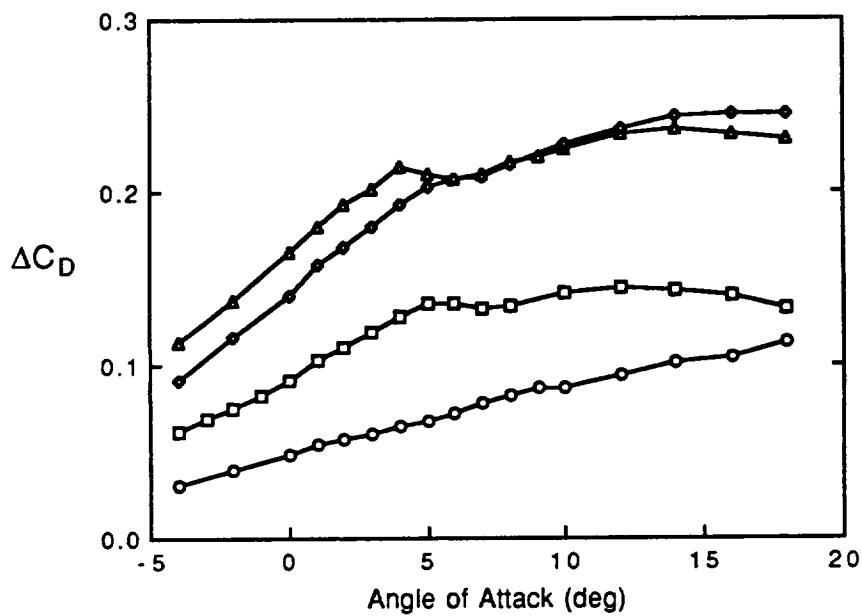
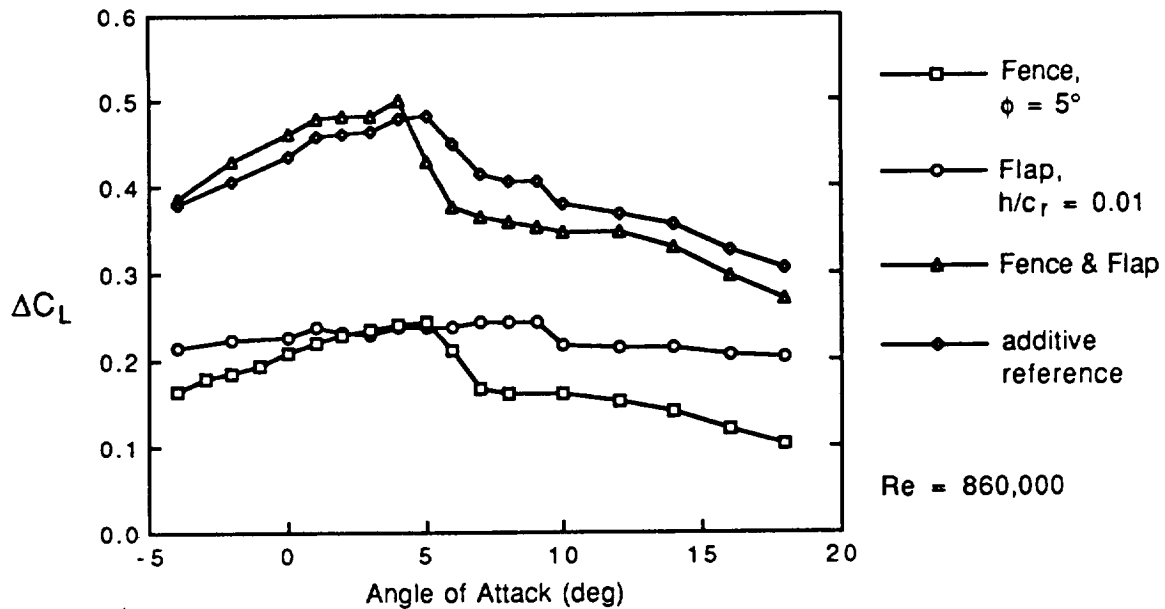


Figure 33. Gain in Lift and Drag for Combined Fence-Flap Configuration.

## REFERENCES

1. Rossow, V.J., "Lift Enhancement by an Externally Trapped Vortex," Journal of Aircraft, Vol. 15, No. 9, Sept. 1978, pp. 618-625.
2. Rossow, V.J., "Aerodynamics of Airfoils with Vortex Trapped by Two Spanwise Fences," AIAA Paper No. 91-3269, 1991.
3. Rossow, V.J., "Two-Fence Concept for Efficient Trapping of Vortices on Airfoils," Journal of Aircraft, Vol. 29, No. 5, Sept.-Oct. 1992, pp. 847-855.
4. Riddle, T.W.; Wadcock, A.; Tso, J.; and Cummings, R.M., "Experimental Analysis of Vortex Trapping Techniques," AIAA Paper No. 91-3271, 1991.
5. Buchholz, M.D., Hendrickson, H.C., and Westra, B.W.; "Two-Fence Vortex Trapping on a Low Angle-of-Attack Wing," Senior Project Report, Cal Poly, San Luis Obispo, 1991.
6. Marchman, J.F., "Aerodynamics of Inverted Leading-Edge Flaps on Delta Wings," Journal of Aircraft, Vol. 18, No. 12, Dec. 1981, pp. 1051-1056.
7. Hoffler, K.D.; Rao, D.M.; and Frassinelli, M.C.; "Basic Studies on Delta Wing Flow Modifications by Means of Apex Fences," NASA TM N86-27199, 1986, pp. 203-217.
8. Wahls, R.A., Vess, R.J., and Moskovitz, C.A., "Experimental Investigation of Apex Fence Flaps on Delta Wings," Journal of Aircraft, Vol. 23, No. 10, Oct. 1986, pp. 789-797.
9. Liebeck, R.H., "Design of Subsonic Airfoils for High Lift," Journal of Aircraft, vol. 15, no. 9, Sept. 1978, pp. 547-561.
10. Neuhart, D.H., and Pendergraft Jr., O.C., "A Water Tunnel Study of Gurney Flaps," NASA TM 4071, 1988.

11. Jang, C. S., Ross, J.C., and Cummings, R.M., "Computational Evaluation of an Airfoil with a Gurney Flap," AIAA Paper No. 92-2708-CP, 1992, pp. 801-809.
12. Katz, J., and Largman, R., "Effect of 90 Degree Flap on the Aerodynamics of a Two-Element Airfoil," Journal of Fluids Engineering, Vol. 111, March 1989, pp. 93-94.
13. Hummel, D., and Srinivasan, P.S., "Vortex Breakdown Effects on the Low-speed Aerodynamic Characteristics of Slender Delta Wings in Symmetrical Flow," Journal of the Royal Aeronautical Society, Vol. 71, April 1967, pp. 319-322.
14. Wentz Jr., W.H., and Kohlman, D.L., "Vortex Breakdown on Slender Sharp-Edged Wings," Journal of Aircraft, Vol. 8, No. 3, March 1971, pp. 156-161.
15. Lambourne, N.C., and Bryer, D.W., "The Bursting of Leading-Edge Vortices—Some Observations and Discussion of the Phenomenon," Aero. Res. Council, R&M No. 3070, 1955.
16. Sarpkaya, T., "Vortex Breakdown in Swirling Conical Flows," AIAA Journal, vol. 9, no. 9, Sept. 1971, pp. 1792-1798.
17. Sarpkaya, T., "Effect of the Adverse Pressure Gradient on Vortex Breakdown," AIAA Journal, vol. 12, no. 5, May 1974, pp. 602-607.